

Critical Phenomena in Causal Dynamical Triangulations

J. Ambjørn^{a,b}, D. Coumbe^a, J. Gizbert-Studnicki^c, A. Görlich^c, and J. Jurkiewicz^c

^aThe Niels Bohr Institute, Copenhagen University,
Blegdamsvej 17, DK-2100 Copenhagen Ø, Denmark.
E-mail: ambjorn@nbi.dk, daniel.coumbe@nbi.ku.dk.

^bIMAPP, Radboud University,
Nijmegen, PO Box 9010, The Netherlands.

^cThe M. Smoluchowski Institute of Physics, Jagiellonian University,
Lojasiewicza 11, Kraków, PL 30-348, Poland.
Email: jakub.gizbert-studnicki@uj.edu.pl, andrzej.goerlich@uj.edu.pl, jerzy.jurkiewicz@uj.edu.pl.

(Dated: March 19, 2020)

Abstract

Four-dimensional CDT (causal dynamical triangulations) is a lattice theory of geometries which one might use in an attempt to define quantum gravity non-perturbatively, following the standard procedures of lattice field theory. Being a theory of geometries, the phase transitions which in usual lattice field theories are used to define the continuum limit of the lattice theory will in the CDT case be transitions between different types of geometries. This picture is interwoven with the topology of space which is kept fixed in the lattice theory, the reason being that “classical” geometries around which the quantum fluctuations take place depend crucially on the imposed topology. Thus it is possible that the topology of space can influence the phase transitions and the corresponding critical phenomena used to extract continuum physics. In this article we perform a systematic comparison between a CDT phase transition where space has spherical topology and the “same” transition where space has toroidal topology. The “classical” geometries around which the systems fluctuate are very different in the two cases, but we find that the order of phase transition is not affected by this.

PACS numbers: 04.60.Gw, 04.60.Nc

1 Introduction

Quantum gravity is the attempt to consistently describe gravity as a quantum field theory. Such a description is expected for a number of reasons, including the fact that the other fundamental interactions have all been successfully formulated as quantum field theories. However, treating general relativity, our best description of gravity, as a perturbative quantum field theory spawns a proliferation of divergences at high energies that cannot be removed using standard renormalization techniques [1, 2]. Thus, at least the simplest attempt at quantum gravity is known to fail.

Since the usual perturbative procedure does not work for gravity, a generalised nonperturbative approach has gained traction in recent years, in which couplings are not required to be small or tend to zero in the high-energy limit, but are only required to approach a finite constant. The scale dependence of couplings, as dictated by the renormalization group, must then approach a fixed point at high energies that is precisely scale-invariant, which by construction guarantees a constant limit. This nonperturbative approach to quantum gravity is known as the asymptotic safety scenario [3]. In particular, the so-called exact renormalization group approach has been used to calculate an effective action of quantum gravity and search for non-perturbative fixed points [4]. However, the actual calculations using the exact renormalisation group always includes a truncation of the effective action and it makes reliably establishing the existence of a high-energy fixed point difficult. This motivates a complementary lattice approach, where the fixed point would appear as a continuum limit that can be studied with controlled systematic errors. Studying quantum gravity on the lattice thus provides a powerful complementary tool for testing the asymptotic safety scenario.

To date the most successful lattice formulation of quantum gravity is that of causal dynamical triangulations (CDT),¹ at least in the sense that it has a rich phase structure where some of the transitions might be second order transitions which potentially can be used to define continuum limits. Of course, even the existence of a continuum limit does not ensure that the continuum theory is (a quantum version of) general relativity. It has to be proven, but a discussion of whether or not that is the case will not be a topic of this article².

In CDT continuous spacetime is approximated by a network of locally flat d -dimensional triangles subject to a causality condition, in which the lattice is foliated into space-like hypersurfaces each with a fixed topology. Using Regge calculus [7] one can write a discretised Einstein-Hilbert action in terms of bulk variables associated with the lattice regularisation for a given CDT triangulation as

$$S_{EH} = -(\kappa_0 + 6\Delta)N_0 + \kappa_4(N_{4,1} + N_{3,2}) + \Delta(2N_{4,1} + N_{3,2}), \quad (1)$$

where $N_{i,j}$ denotes the number of 4-dimensional simplicial building blocks with i vertices on hypersurface t and j vertices on hypersurface $t+1$, and N_0 is the number of vertices in the triangulation. κ_0 , Δ and κ_4 are bare coupling constants. κ_0 and κ_4 are related to Newton's constant and the cosmological constant, respectively, and Δ defines the ratio of the length of space-like and time-like links on the lattice. The parameter κ_4 , which is proportional to the cosmological constant, is tuned such that one can take an infinite-volume limit.

There are two varieties of elementary building blocks in CDT, the (4, 1) and (3, 2) simplices [6]. The local Monte Carlo moves used in CDT simulations do not always preserve the numbers $N_{4,1}$ and $N_{3,2}$ of these building blocks, or their sum. However, the total system volume can be controlled by a volume-fixing term

$$\delta V = \epsilon(N_{4,1} - N_4^{\text{target}})^2, \quad (2)$$

such that it is sharply peaked about a chosen value, with a well-defined range of fluctuations. N_4^{target} is the chosen target volume about which it fluctuates, and ϵ is a numerical constant that controls the magnitude of volume fluctuations. Prior to starting numerical simulations one has the freedom to fix either the total number of 4-dimensional simplicial building blocks $N_4 = N_{4,1} + N_{3,2}$

¹For the original articles see [5], for a review [6].

²Since CDT has a built in time foliation, it has been argued [19] that a natural continuum limit could also be a version of Horava-Lifshitz gravity [20].

or just the number of $N_{4,1}$ simplices, where the latter volume fixing is often chosen merely for technical convenience.

In CDT simulations, the fixed topology of spatial slices and that of the proper time axis must be chosen from the outset. The vast majority of CDT Monte Carlo simulations have been performed with the spatial topology of a three-sphere S^3 , and the temporal topology of S^1 , yielding a global spacetime topology $\mathcal{T} = S^3 \times S^1$. However, one is not only restricted to spherical topology. In fact, one is free to choose any suitable topology (see [9] for a recent study of CDT with toroidal topology).

Since κ_4 is tuned to its critical value in the simulations, the only parameters that need to be varied in order to explore the CDT parameter space are κ_0 and Δ . The CDT parameter space has now been studied fairly extensively, with the central features depicted in Fig. 1. Phases *A* and *B* have geometrical properties that make them unlikely to model our macroscopic universe, and are typically thought to be lattice artifacts. Phase C_b is the recently discovered bifurcation phase, with a number of peculiar geometric features (see [10, 11, 12, 13, 14] for more details). Phase *C* is the physically interesting phase of CDT, since it exhibits a semiclassical geometry that closely resembles Euclidean de Sitter space in 4-dimensions at large distances [6, 15].

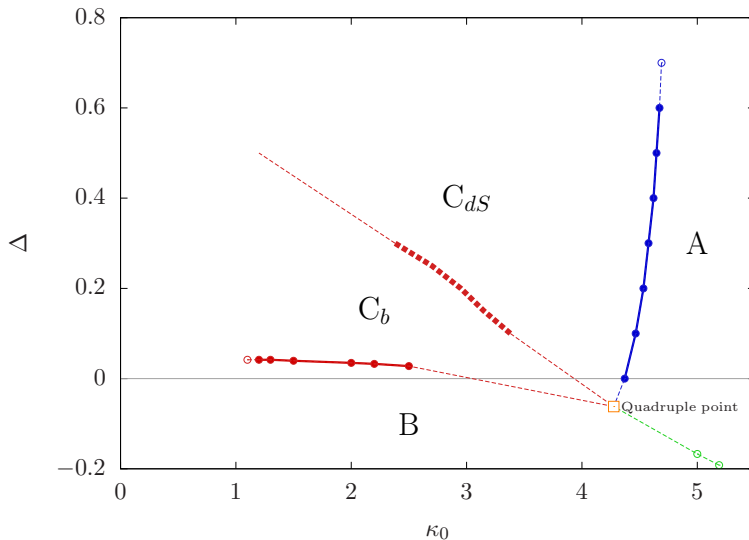


Figure 1: The phase structure of 4-dimensional CDT.

There exist a number of previous studies on the phase transition lines bordering the physically interesting phase *C*. The transition between phases *A* and *C* was found to be almost certainly first order, while the *B* – C_b transition likely second order [16, 17]. A recent study also found the *C* – C_b transition to be a likely second order transition [13]. Definitively establishing the order of all transitions in the CDT parameter space is important since proving the existence of a second order transition may establish a continuum limit and facilitate contact with the asymptotic safety scenario [18].

However, given the freedom in how the numerical CDT simulations can be setup, such as the topology of each spatial slice, the number of time slices and the particular volume-fixing method, we want to investigate the possible impact that these variables may have on CDT phase transitions. In this work, we therefore explore the potential impact topology, time slicing and volume-fixing may have on critical phenomena in CDT. Here, we restrict our attention to the *A* – *C* transition only, since numerical Monte Carlo simulations run relatively fast in this part of the parameter

space which makes the large data collections needed for such a study more feasible. The lessons learnt from this study are expected to aid investigations of other CDT transitions in future works.

In order to facilitate Monte Carlo simulations near the phase transition, we tested a new numerical code aimed at decreasing autocorrelation time of the measured data for some systems. This code is based on the so-called parallel tempering/replica exchange method. The technical details of this new code will be published elsewhere.

2 Order parameters and observables

Phase transitions are usually triggered by breaking of some symmetry. The symmetry difference between the disordered and the ordered phase can be captured by an order parameter OP , which is usually zero (or constant) in the disordered phase and changes (usually rises) in the ordered phase. There is some freedom in defining an order parameter and thus order parameters should be tailored to the nature of a given phase transition. The choice of a "good" order parameter is especially important in numerical studies, such as Monte Carlo simulations used to investigate Causal Dynamical Triangulations.

In the numerical study of four-dimensional CDT, one defines the pseudo-critical points by looking for peaks in the susceptibility

$$\chi_{OP} \equiv \langle OP^2 \rangle - \langle OP \rangle^2, \quad (3)$$

within the (κ_0, Δ) parameter space. As can be seen in the phase diagram of Fig. 1 the A - C transition line is almost parallel with the Δ -axis, thus one usually fixes Δ and measures χ_{OP} as a function of κ_0 , looking for a maximum in χ_{OP} at κ_0^{crit} (see e.g. Fig. 7). Typically, the position of the pseudo-critical points moves in the parameter space when the system size is increased. Therefore, in order to quantify finite size effects, one measures systems with higher and higher lattice volume $N_{4,1}$ (or alternatively N_4 , depending on the volume fixing method). One then performs a finite size scaling analysis by fitting the power-law behaviour

$$\kappa_0^{crit}(N_{4,1}) = \kappa_0^{crit}(\infty) - CN_{4,1}^{-\frac{1}{\gamma}}, \quad (4)$$

where $\kappa_0^{crit}(N_{4,1})$ is the pseudo-critical value for a finite system size $N_{4,1}$, $\kappa_0^{crit}(\infty)$ is the true critical value in the infinite volume limit and C is a constant of proportionality. A critical exponent of $\gamma = 1$ indicates a first order transition, while $\gamma > 1$ suggests a higher order transition.

One can also analyse the behaviour of the order parameter OP measured at the pseudo-critical point κ_0^{crit} . First order transitions are usually characterised by two distinct metastable states of OP and thus the order parameter jumps (in the Monte Carlo simulation time) between the two states, which can be observed as two separate peaks in the measured OP histograms (see e.g. Fig. 8). For a first order transition, the probability of tunnelling between the two states should decrease when the lattice volume $N_{4,1}$ increases, and thus the two peaks should become easier to distinguish. At some lattice size, the separation of the peaks is so large (relative to the amplitude of fluctuations within a single peak) that the jumps of the OP between the metastates are suppressed such that the system gets frozen in one of the metastates and one observes hysteresis around the critical point. If instead, the transition is second (or higher) order then only one state is present, and thus only one peak in the OP histogram is observed at the critical point.³ The critical point is then

³In some cases, e.g. for the B - C_b phase transition [17, 16], one could observe the appearance of two metastates also for a higher order transition measured for finite lattice sizes, but the separate peaks would merge into a single peak in the infinite volume limit. The reason for this atypical behaviour was analysed in detail in [14].

OBSERVABLE	1st order transition	Higher order transition
OP histograms measured at pseudo-critical points κ_0^{crit}	double peaks peak separation \uparrow with $N_{4,1} \rightarrow \infty$	single peak or peaks merging with $N_{4,1} \rightarrow \infty$
Pseudo-critical point scaling $\kappa_0^{crit}(N_{4,1})$, eq. (4)	γ $= 1$	γ > 1
Binder cumulant (5) scaling at pseudo-critical points κ_0^{crit}	$B_{OP}^{min}(N_{4,1} \rightarrow \infty)$ < 0	$B_{OP}^{min}(N_{4,1} \rightarrow \infty)$ $= 0$

Table 1: Characteristics of the first and the higher order phase transitions.

characterised by the maximal amplitude of OP fluctuations, which is captured by the maximum of the susceptibility $\chi_{OP}(\kappa_0)$ observed at κ_0^{crit} .

Another quantity of interest is the Binder cumulant⁴

$$B_{OP} \equiv \frac{1}{3} \left(1 - \frac{\langle OP^4 \rangle}{\langle OP^2 \rangle^2} \right), \quad (5)$$

which (similar to χ_{OP}) can be used to find the position of the A - C phase transition line. In this case, pseudo-critical points are signalled by local minima of B_{OP} in the (κ_0, Δ) parameter space. Again, one defines the A - C pseudo-critical points by fixing Δ and analyses B_{OP} as a function of κ_0 looking for minima appearing at κ_0^{crit} . The result will again depend on lattice volume and one can use equation (4) to estimate the $\kappa_0^{crit}(\infty)$ and the critical exponent γ , and it is believed that finite size effects are smaller compared to the susceptibility method discussed above. One can also look at scaling of the (minimum) level of B_{OP} measured at the phase transition point:

$$B_{OP}^{min} \equiv B_{OP}(\kappa_0^{crit}). \quad (6)$$

For a first order transition, where the OP histograms measured at the critical point κ_0^{crit} have two shifted peaks, the $B_{OP}^{min}(N_{4,1} \rightarrow \infty)$ will move away from zero as the two peaks become more and more apparent when the histograms approach two shifted Dirac-delta functions placed at positions of the peaks' centres. If instead, the transition is second (or higher) order, then the histograms have only one peak and $B_{OP}^{min}(N_{4,1} \rightarrow \infty)$ should tend to zero.

The above observables and their characteristic behaviour for the first and the higher order transitions are summarised in Table 1.⁵

In a previous study of the A - C transition in CDT with spherical spatial topology [17] and in a recent paper about the phase structure of CDT with toroidal spatial topology [22], a number

⁴Note that here we use a definition of the Binder cumulant which is shifted (by a $-2/3$ constant) versus the original Binder's formulation [21]: $B_x = 1 - \frac{1}{3} \frac{\langle x^4 \rangle}{\langle x^2 \rangle^2}$. The definition (5) was also used in previous CDT phase transition studies [17] and thus we keep it in order to ease comparison with these results. The virtue of using our definition is that, as explained in the text, the deviation of (critical) B_{OP} from zero with rising lattice volume may signal a first order transition, while the convergence to zero is characteristic of a higher order transition. One could as well use the original Binder's definition and look at the deviation from $2/3$.

⁵One could also analyse scaling of $\chi_{OP}^{max} \equiv \chi_{OP}(\kappa_0^{crit})$, but χ_{OP} and B_{OP} are strongly related (see e.g. Eqs. (10) and (11)) and thus one can focus just on the latter. Another possibility is to check the connected Binder cumulant $B_{OP}^c \equiv \frac{1}{3} \left(1 - \frac{\langle (OP - \langle OP \rangle)^4 \rangle}{\langle (OP - \langle OP \rangle)^2 \rangle^2} \right)$. $B_{OP}^c(N_{4,1} \rightarrow \infty)$ measured at the transition point should tend to zero for a first order transition and, as a consequence of the positive kurtosis in the OP probability distribution at the higher order transition, it should be deflected from zero for the higher order transition. Unfortunately, this quantity does not give any statistically significant signals for the data discussed.

of order parameters were defined and used to study the phase transition in question. They were mainly related to very global properties of triangulations, such as the (extensive) total number of vertices N_0 or the (intensive) ratios $OP_1 \equiv \frac{N_0}{N_4}$ and $OP_2 \equiv \frac{N_{3,2}}{N_{4,1}}$. In fact, when one couldn't observe the phase transition signal using OP , one could try to use some monotonic functions of the above order parameters, e.g. $f(OP) = \sqrt{OP}$ or $f(OP) = \ln OP$. Such a choice was useful when an order parameter was changing by a few orders of magnitude at the phase transition, as used in Ref. [22].

Now, we want to choose "the best" order parameters (or their monotonic functions) giving the strongest signal-to-noise ratios irrespective of the simulation details, i.e. the ones being "critical" no matter how we choose the topology, time slicing or the volume-fixing method. Specifically, we will analyse the susceptibility (3) or the Binder cumulant (5) in search of extrema ($\chi_{OP}(\kappa_0)$ maxima or $B_{OP}(\kappa_0)$ minima) in the transition region. We therefore define "criticality" via the existence of such extrema. For each OP considered, we first check the "criticality" of OP and, if it is not observed, we also check the "criticality" of \sqrt{OP} and $\ln(OP)$ both for the susceptibility and the Binder cumulant. In fact, one may show that these quantities are strongly dependent if the order parameter's fluctuations are relatively small compared to its mean value, which seems to be the case in all data analysed herein. In this case, the susceptibility of a function of an order parameter $f(OP)$ is very well approximated by

$$\chi_{f(OP)} \approx (f'(\langle OP \rangle))^2 \chi_{OP}, \quad (7)$$

where f' denotes the derivative of the function f . For the square root and the logarithm one gets (up to a trivial rescaling⁶)

$$\chi_{\sqrt{OP}} \approx \frac{\chi_{OP}}{\langle OP \rangle}, \quad (8)$$

$$\chi_{\ln OP} \approx \frac{\chi_{OP}}{\langle OP \rangle^2}, \quad (9)$$

respectively. Therefore, from (5) and (3), one immediately obtains

$$B_{\sqrt{OP}} = \frac{1}{3} \left(1 - \frac{\langle \sqrt{OP}^4 \rangle}{\langle \sqrt{OP}^2 \rangle^2} \right) = -\frac{1}{3} \left(\frac{\langle OP^2 \rangle - \langle OP \rangle^2}{\langle OP \rangle^2} \right) = -\frac{1}{3} \frac{\chi_{OP}}{\langle OP \rangle^2} \approx -\frac{1}{3} \chi_{\ln OP},$$

and so (at least up to a rescaling)

$$B_{\sqrt{OP}} \approx -\chi_{\ln OP}. \quad (10)$$

One can also empirically check that in all cases analysed the maxima of $\chi_{\sqrt{OP}}$ coincide with the minima of $B_{\ln OP}$, i.e. the position of the critical κ_0^{crit} based on these extrema is identical, although the extremal values are different (cannot be matched by a trivial rescaling) - which we denote via

$$\chi_{\sqrt{OP}} \sim -B_{\log OP}. \quad (11)$$

In a sense the functions \sqrt{OP} and $\ln OP$ used to compute the susceptibility and the Binder cumulant are "conjugate" to each other, and thus it is enough to look at one of them, e.g. \sqrt{OP} . By assuming small OP fluctuations (relative to $\langle OP \rangle$) and using equations (10) and (7) one can easily show that

$$B_{OP} \approx -\chi_{\ln OP^2} = -\chi_{2 \ln OP} \approx -4\chi_{\ln OP} \approx 4B_{\sqrt{OP}},$$

⁶In fact $\chi_{\sqrt{OP}} \approx \frac{1}{4} \frac{\chi_{OP}}{\langle OP \rangle}$.

so again (up to a rescaling)

$$B_{\sqrt{OP}} \approx B_{OP}. \quad (12)$$

Consequently, the susceptibilities and Binder cumulants of \sqrt{OP} capture the most important information encoded in our data and thus we will focus on that function if we cannot get the phase transition signal for the OP itself.

The question remains, which of the proposed order parameters N_0 , $OP_1 \equiv \frac{N_0}{N_4}$ or $OP_2 \equiv \frac{N_{3,2}}{N_{4,1}}$ is best suited for our purposes, i.e. which one is really "critical" independent of the topology, time slicing or the volume-fixing method. To answer this question, in each case we have analysed the behaviour of $\langle OP \rangle$, χ_{OP} and $\frac{\chi_{OP}}{\langle OP \rangle} \approx \chi_{\sqrt{OP}}$. The exemplary results for the toroidal topology with $T = 4$ proper-time period and two different volume fixing methods are presented in Fig. 2, Fig. 3 and Fig. 4.

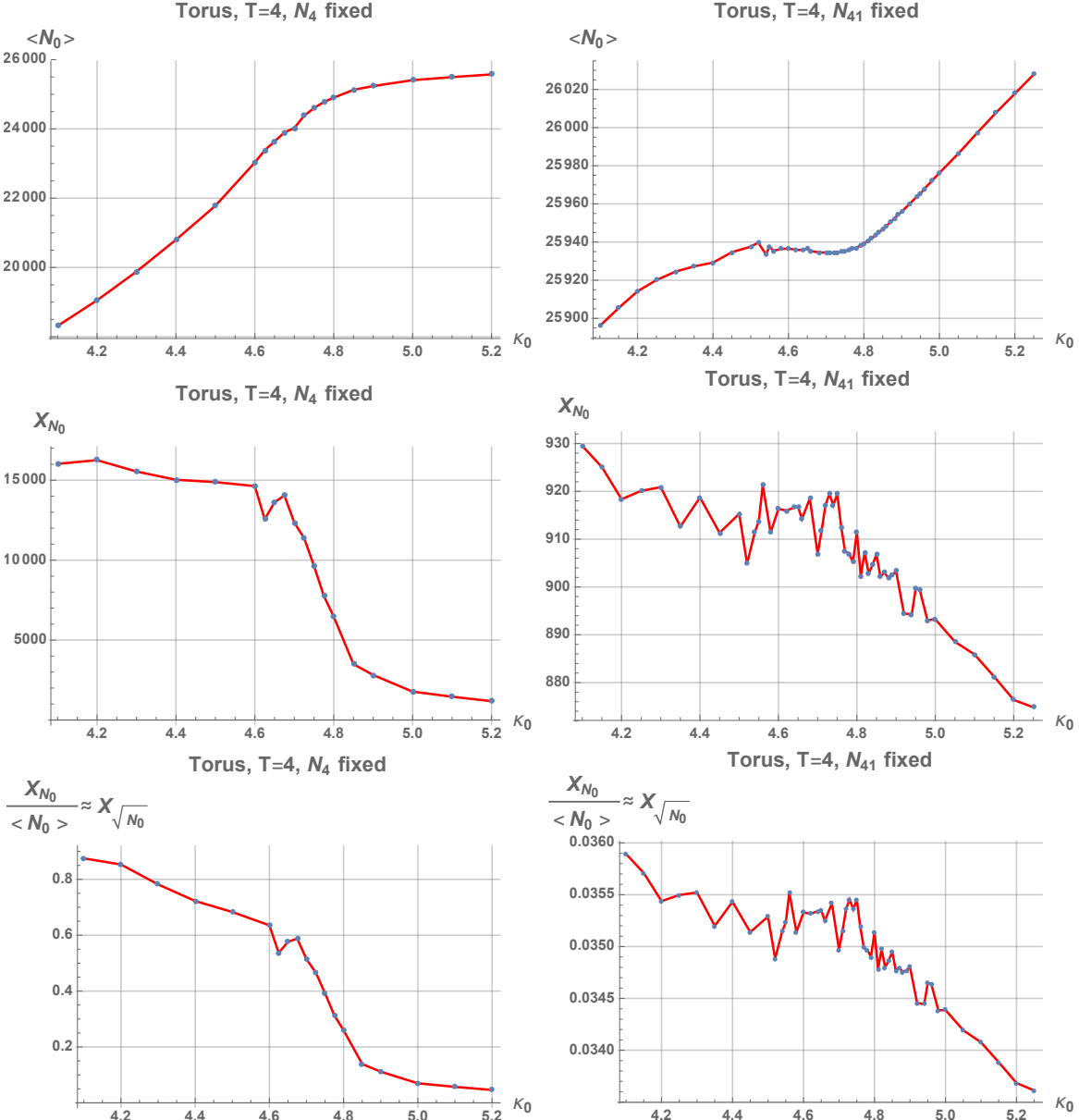


Figure 2: The mean value $\langle OP \rangle$ (top), the susceptibility χ_{OP} (middle) and the susceptibility $\chi_{\sqrt{OP}}$ (bottom) of the order parameter $OP = N_0$ measured near the A - C transition in CDT with toroidal spatial topology and a proper-time period $T = 4$. Left plots are for N_4 volume fixing and right plots are for $N_{4,1}$ volume fixing. None of the susceptibility plots shows "critical" behaviour.

Let us start with the $OP = N_0$, which was used in the original study of the A - C phase transition performed for spherical spatial topology [17] where the A - C transition was shown to be first-order. The analysis was done with the total N_4 volume fixed and for a time period of $T = 80$. In this case, the order parameter $\langle N_0 \rangle$ was constant in the "disordered" A phase (appearing at large κ_0) and decreased in the "ordered" C phase (appearing at smaller κ_0).⁷ The same type of $\langle N_0 \rangle$ behaviour is observed in toroidal CDT with $T = 4$ time slices when N_4 is fixed - see Fig. 2 (left), but this

⁷For the A - C transition, phase A can be treated as the "disordered" and phase C as the "ordered" one. We use these words in analogy with the Ising spin system where the spins fluctuate around a minimum of the Hamiltonian in the ordered phase, while they fluctuate around zero in the disordered phase. In phase C the geometries fluctuate around a non-trivial "classical" solution, which in the case where the spatial topology is S^3 has the form of S^4 with

is no longer the case when one chooses to fix $N_{4,1}$ - see Fig. 2 (right). In the latter case $\langle N_0 \rangle$ is also increasing in phase A , although there is some visible inflection point occurring at the A - C phase transition. The order parameter was definitely "critical" in the spherical topology [17] but it seems not to be "critical" in the toroidal CDT case, where one cannot observe any statistically significant peaks in the susceptibility χ_{N_0} or in $\frac{\chi_{N_0}}{\langle N_0 \rangle} \approx \chi_{\sqrt{N_0}}$ for any volume fixing method.

a "stalk" of cut off size in the spatial directions connecting the north and south pole of S^4 in the time direction, and making the topology compatible with $S^1 \times S^3$ rather than S^4 (see [6] for details and Fig. 42 for a plot of the spatial volume profile, including the stalk). This "classical" solution breaks translational symmetry, which is restored when the motion of the centre of mass of the S^4 part of the geometry in the S^1 time direction is included. This is in contrast to the situation in phase A where the spatial volumes at different times seems to fluctuate around the "trivial" mean value $N_{4,1}/T$.

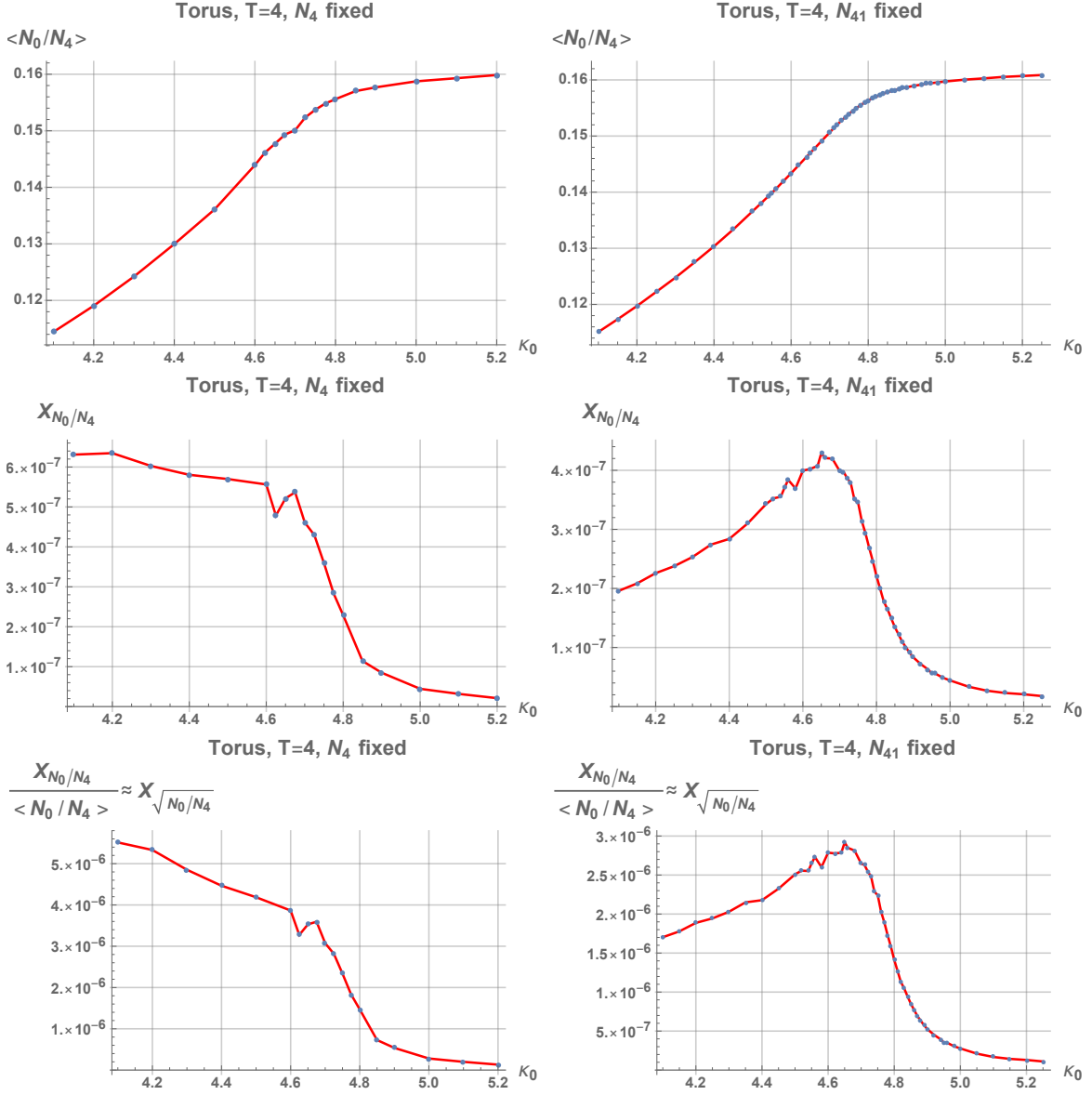


Figure 3: The mean value $\langle OP \rangle$ (top), the susceptibility χ_{OP} (middle) and the susceptibility $\chi_{\sqrt{OP}}$ (bottom) of the order parameter $OP_1 \equiv \frac{N_0}{N_4}$ near the A - C transition in CDT with toroidal spatial topology and a $T = 4$ proper-time period. Left plots are for N_4 volume fixing and the right plots are for $N_{4,1}$ volume fixing. The susceptibility plots seem to show "critical" behaviour for $N_{4,1}$ volume fixing but the order parameter is not "critical" when N_4 is fixed.

The situation looks better if one chooses to use the (intensive) $OP = OP_1 \equiv \frac{N_0}{N_4}$. This was obviously "critical" in the original study [17] of spherical CDT, when N_4 was kept fixed. OP_1 again is *not* "critical" in the toroidal case for the same volume fixing method - see Fig. 3 (left) - but it seems to be "critical" for toroidal CDT with $N_{4,1}$ fixed - see Fig. 3 (right), where one can observe peaks both for χ_{OP_1} and $\chi_{\sqrt{OP_1}}$.

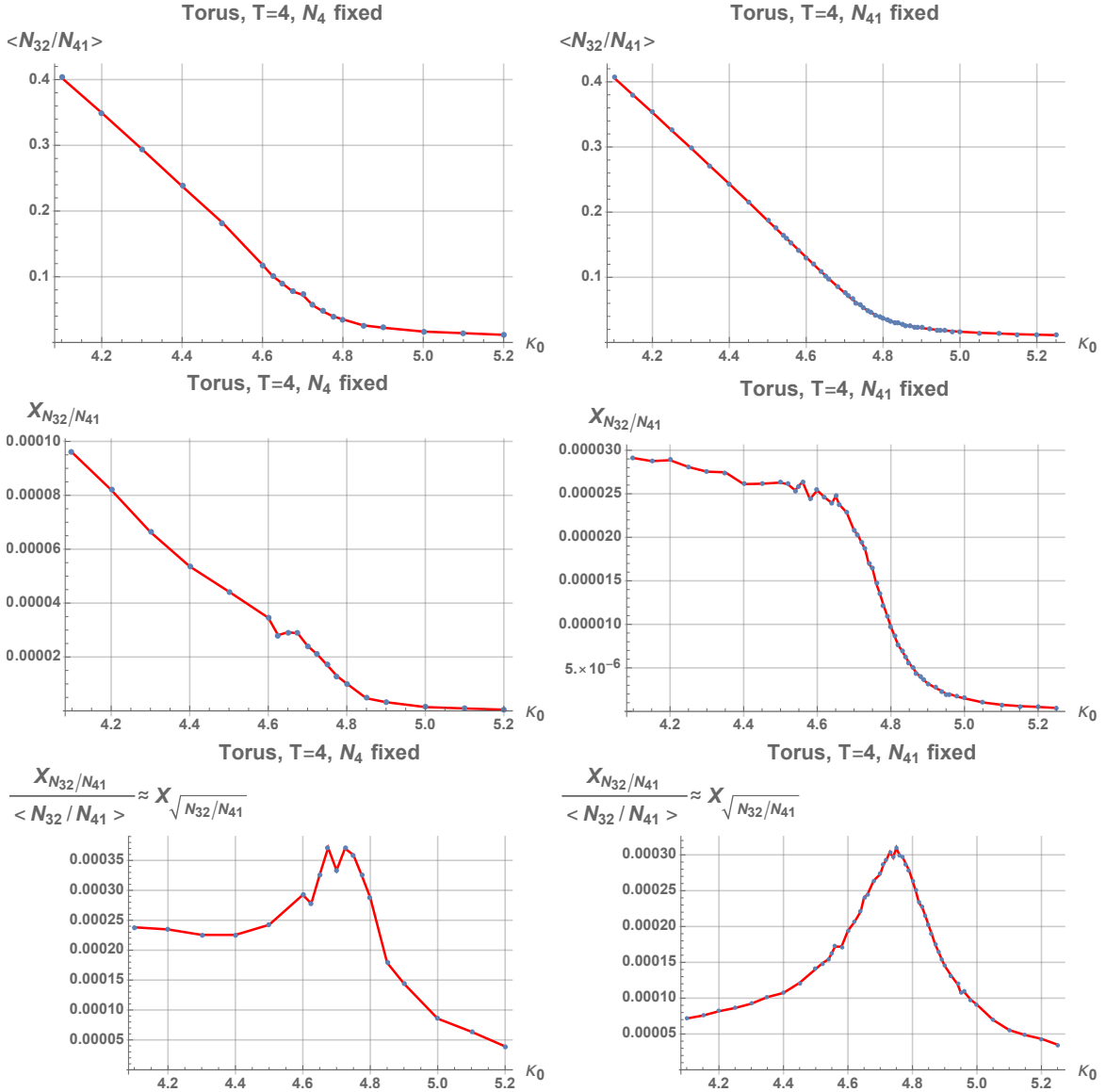


Figure 4: The mean value $\langle OP \rangle$ (top), the susceptibility χ_{OP} (middle) and the susceptibility $\chi_{\sqrt{OP}}$ (bottom) of the order parameter $OP_2 \equiv \frac{N_{3,2}}{N_{4,1}}$ measured near the A - C transition in CDT with toroidal spatial topology and a $T = 4$ proper-time period. Left plots are for N_4 volume fixing and the right plots are for $N_{4,1}$ volume fixing. $\chi_{\sqrt{OP}}$ shows "critical" behaviour in all cases analysed.

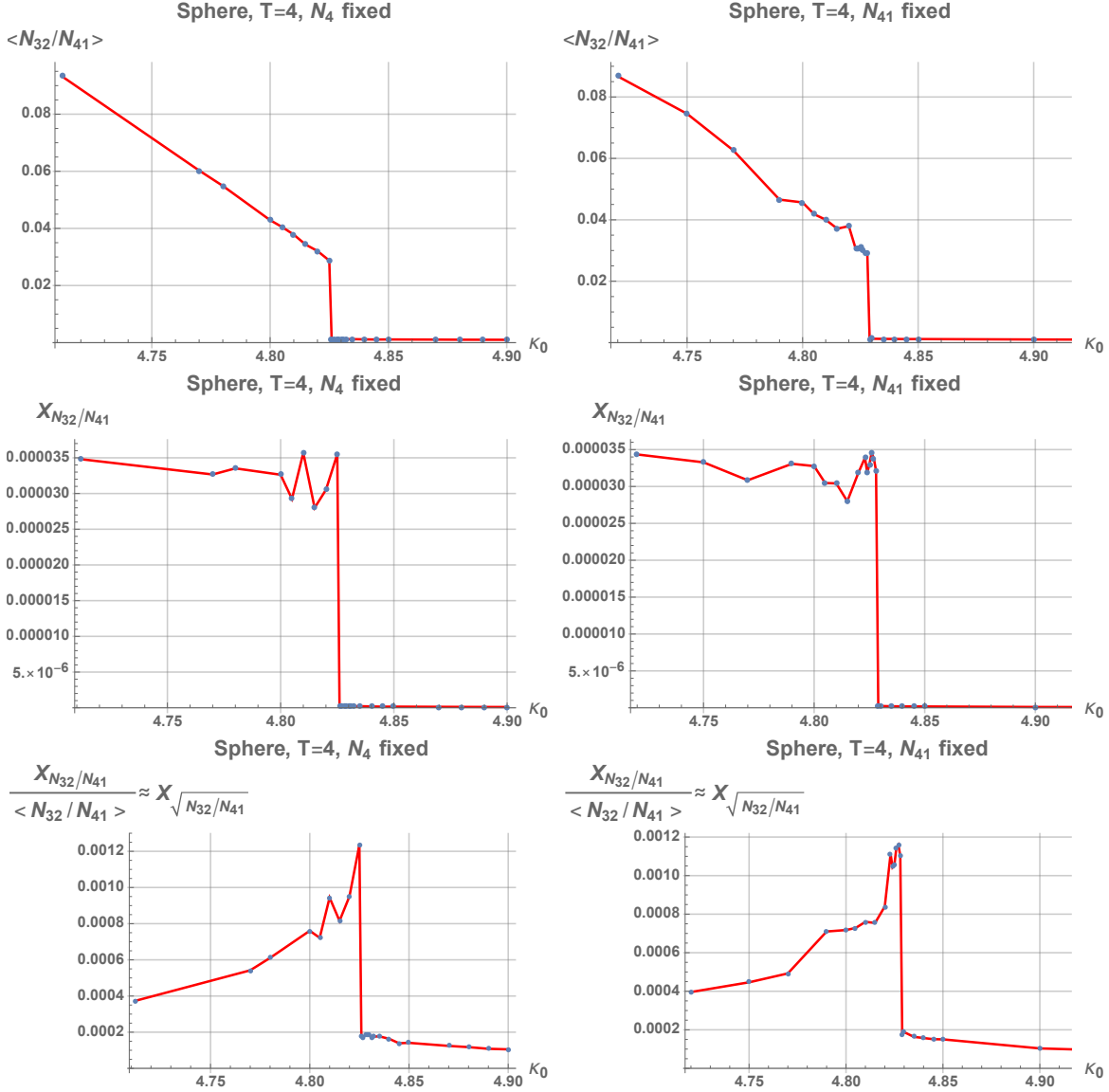


Figure 5: The mean value $\langle OP \rangle$ (top), the susceptibility χ_{OP} (middle) and the susceptibility $\chi_{\sqrt{OP}}$ (bottom) of the order parameter $OP_2 \equiv \frac{N_{3,2}}{N_{4,1}}$ measured near the A - C transition in CDT with spherical spatial topology and a $T = 4$ proper-time period. Left plots are for N_4 fixed and the right plots are for $N_{4,1}$ fixed. Both χ_{OP} and $\chi_{\sqrt{OP}}$ show "critical" behaviour in all cases analysed.

As already discussed, the N_0 susceptibility χ_{N_0} does not show any critical behaviour for any volume fixing method for the toroidal CDT case, so the observed peak in susceptibility $\chi_{\frac{N_0}{N_4}}$ cannot come from N_0 but from $N_4 = N_{4,1} + N_{3,2}$ fluctuations. For fixed $N_{4,1}$, the only fluctuations possible are for $N_{3,2}$, which can be quantified by the ratio $OP_2 \equiv \frac{N_{3,2}}{N_{4,1}}$. This order parameter (or, more precisely, its function $\sqrt{OP_2} \equiv \sqrt{\frac{N_{3,2}}{N_{4,1}}}$) is *truly critical* in all cases analysed here - see Fig. 4 and Fig. 5, where we plot the data for $T = 4$ time slices for the toroidal and the spherical spatial topology, respectively. Similar results were also obtained for larger T . In fact one can show that the spurious "criticality" of $OP_1 \equiv \frac{N_0}{N_4}$, observed for toroidal CDT when $N_{4,1}$ was fixed, is illusory and can be explained by the behaviour of the "truly critical" $\sqrt{OP_2}$. For fixed $N_{4,1} = \bar{N}_{4,1}$, assuming constant

$N_0 \approx \langle N_0 \rangle$ and using the small fluctuations approximation (7) one has

$$\chi_{\frac{N_0}{N_4}} \approx \chi_{\frac{\langle N_0 \rangle}{\bar{N}_{4,1} + N_{3,2}}} = \chi_{\frac{\langle N_0 \rangle}{\bar{N}_{4,1}}} (1 + \sqrt{OP_2})^{-1} \approx \left(\frac{2\langle N_0 \rangle \langle \sqrt{OP_2} \rangle}{\bar{N}_{4,1} (1 + \langle \sqrt{OP_2} \rangle)^2} \right)^2 \chi_{\sqrt{OP_2}}. \quad (13)$$

In Figure 6 we again plot the susceptibility $\chi_{\frac{N_0}{N_4}}$ calculated for the toroidal CDT with fixed $N_{4,1}$, the same as in Fig. 3 right, together with its approximation by the susceptibility $\chi_{\sqrt{OP_2}}$ (13) (the dashed-black line). The spurious "criticality" peak of $\chi_{\frac{N_0}{N_4}}$ is perfectly explained by the truly "critical" peak of $\chi_{\sqrt{OP_2}}$ (the green line) multiplied by the prefactor (the dashed-green line).

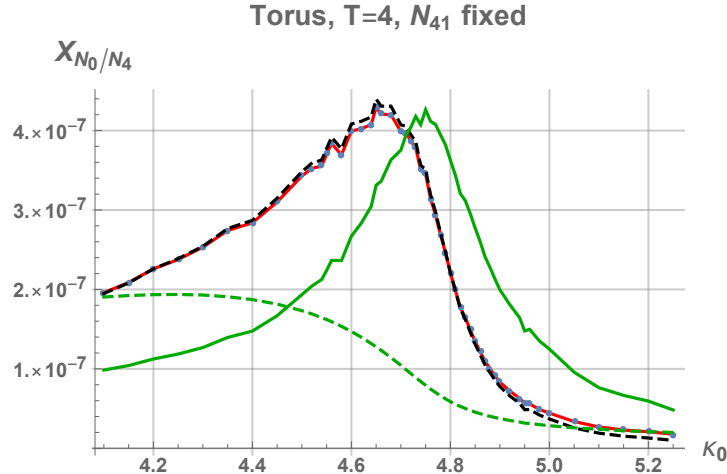


Figure 6: The peak of susceptibility $\chi_{\frac{N_0}{N_4}}$ is perfectly explained by the peak of the "really critical" $\chi_{\sqrt{OP_2}}$ (green line) multiplied by a prefactor of equation (13) (dashed-green line). The (small-fluctuations) approximation (13) is plotted as the dashed-black line and it is very close to the measured $\chi_{\frac{N_0}{N_4}}$ data (red line).

Summing up, among all the order parameters analysed

$$OP_2 \equiv \frac{N_{3,2}}{N_{4,1}}, \quad (14)$$

(or more precisely its function $\sqrt{OP_2}$) shows "truly critical" behaviour irrespective of the topology, time slicing or the volume-fixing method. Therefore, in the following sections we will focus on this order parameter. Specifically, we will try to repeat the results of the previous phase transition study [17] for the spherical spatial topology, originally done using N_0 or $OP_1 \equiv \frac{N_0}{N_4}$, now using OP_2 . We will then investigate the impact of the volume-fixing method ($N_{4,1}$ vs N_4), the time-slicing (large $T = 80$ vs small $T = 4$) and spatial topology (the spherical topology vs the toroidal topology) on our results.

3 Spherical topology

3.1 The order of the A - C transition

The A - C transition in four-dimensional CDT with spherical spatial topology was earlier analysed in Ref. [17] where it was found to likely be a first order transition. The study was based on the

analysis of the N_0 order parameter and using a N_4 volume fixing method applied to triangulations with $T = 80$ time slices. The data showed all characteristics of the first order transition summarised in Table 1, namely one could observe double peaks in the N_0 histograms measured at the pseudo-critical points, the critical exponent of equation (4) was consistent with $\gamma = 1$ and the (minimum of the) Binder cumulant $B_{N_0}^{min}$ was diverging from zero for large lattice volumes $N_4 \rightarrow \infty$ [17].

Now we will use the OP_2 parameter defined in formula (14). Measurements presented in this section were made at $\Delta = 0.6$, for a maximum of 8 different lattice volumes ranging from $N_{4,1} = 20k$ to $N_{4,1} = 160k$ in increments of $20k$ with $T = 80$ time slices. For the $N_{4,1} = 20k$ and $40k$ ensembles a double peak cannot be distinguished from a histogram analysis because the lattice volumes are too small to exhibit clear transitions between metastable phases. However, the pseudo-critical κ_0^{crit} values can still be estimated by finding the maximum in susceptibility χ_{OP_2} of the order parameter as a function of κ_0 (see Fig. 7), albeit with reduced accuracy.⁸

The same procedure of locating the peak in the susceptibility χ_{OP_2} is performed for the larger system sizes, where a full histogram analysis is possible for lattice volumes between $N_{4,1} = 60k$ and $N_{4,1} = 160k$ at the transition points. For system sizes equal to or greater than $N_{4,1} = 60k$ a histogram with a double Gaussian structure is clearly observed for each point, as shown in Fig. 8. The pseudo-critical κ_0^{crit} values at which the transition occurs exhibit a clear volume dependency, with the separation of the double Gaussian peaks becoming more pronounced with increasing system size (see Fig. 8).

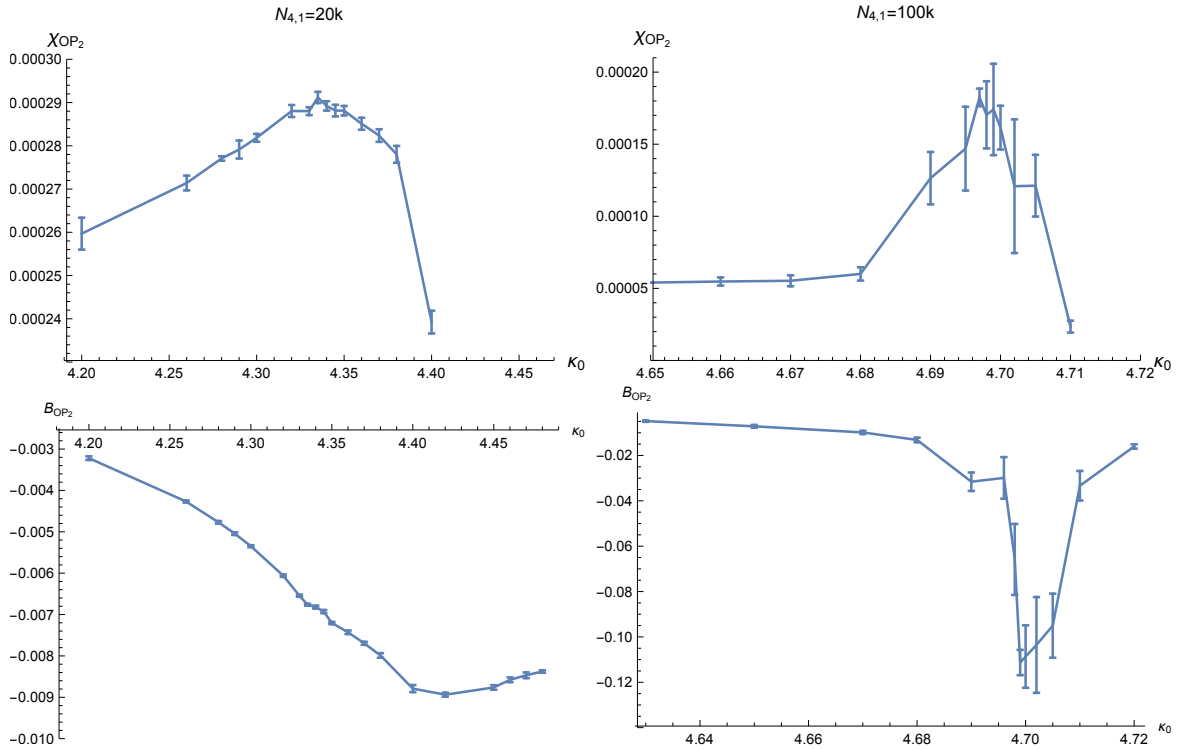


Figure 7: The susceptibility χ_{OP_2} as defined by Eq. (3) (top charts) and the Binder cumulant B_{OP_2} as defined by Eq. (5) (bottom charts) as a function of κ_0 . Left charts are for $N_{4,1} = 20k$ and right charts are for $N_{4,1} = 100k$.

⁸Alternatively, one can look at the maximum of the susceptibility $\chi_{\sqrt{OP_2}}$, which gives similar results to χ_{OP_2} but with a slightly higher pseudo-critical κ_0 value.

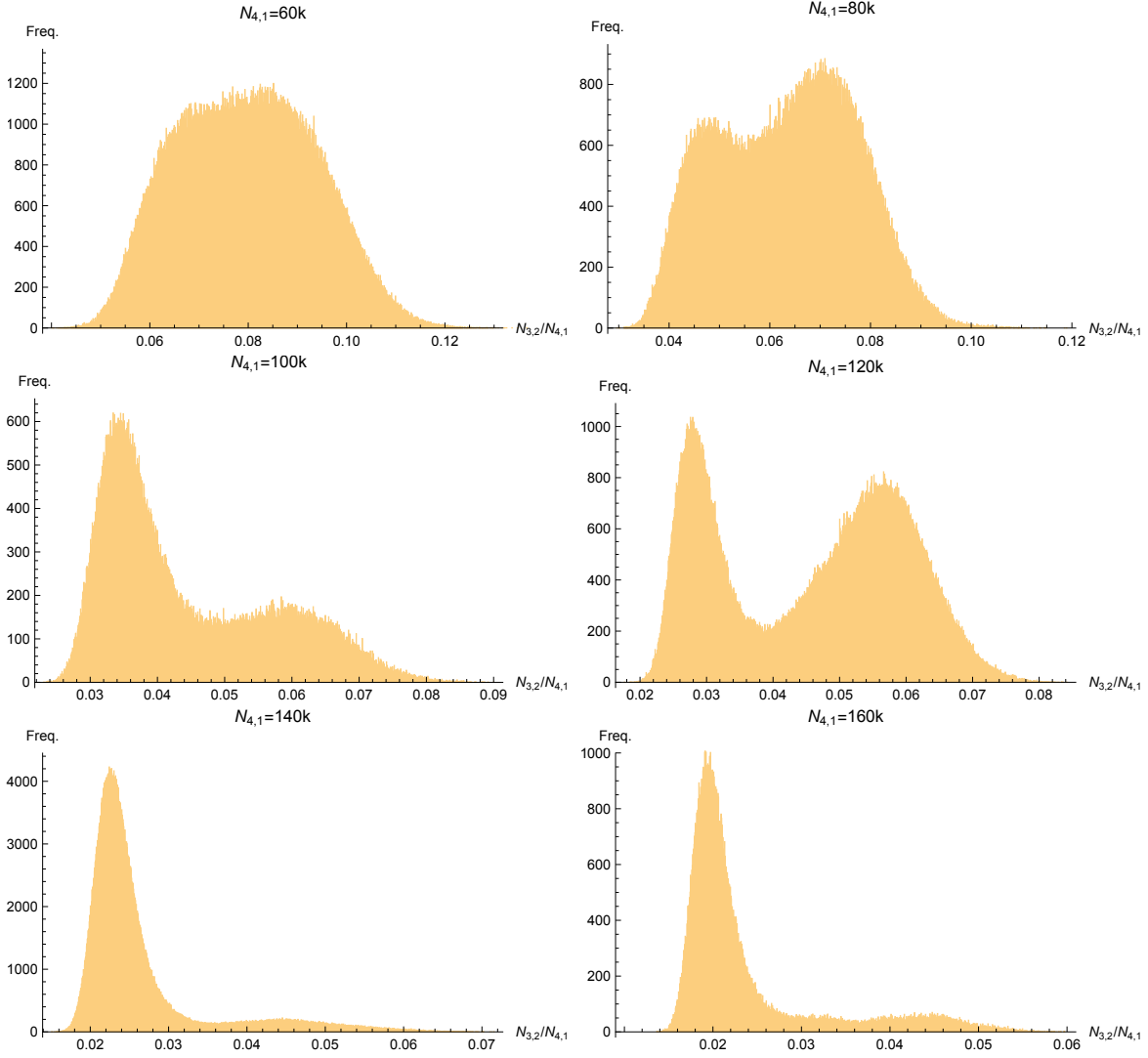


Figure 8: Histogram of $OP_2 \equiv N_{3,2}/N_{4,1}$ at pseudo-critical κ_0^{crit} values for $\Delta = 0.6$ with fixed lattice volumes $N_{4,1} = 60k, 80k, 100k, 120k, 140k, 160k$. The height of the two peaks is not exactly the same as (due to the κ_0 resolution applied) some data were measured slightly away from the real pseudo-critical points.

The order of a given transition can be quantified by the critical exponent γ of Eq.(4) which details how exactly the pseudo-critical values κ_0^{crit} scale with system size. Applying Eq. (4) to κ_0^{crit} defined by the maxima of susceptibility χ_{OP_2} measured for all system sizes (see Fig. 9) yields a shift exponent of $\gamma = 1.16 \pm 0.07$, confirming the likely first order nature of the $C-A$ transition reported previously in Ref. [17].

An alternative method for estimating the critical exponent γ is to determine the pseudo-critical κ_0^{crit} values by locating the minima of B_{OP_2} for different lattice volumes (see Fig. 7). The κ_0^{crit} values determined in this way are shifted to higher values compared with κ_0^{crit} based on peaks in χ_{OP_2} , however this discrepancy appears to reduce for larger lattice volumes (see Fig. 7 and Fig. 9).⁹ Applying Eq. (4) to the κ_0^{crit} values determined by locating the minima of B_{OP_2} yields $\gamma = 1.64 \pm 0.18$, which is statistically inconsistent with $\gamma = 1$.

⁹The minimum of B_{OP_2} could not be determined for $N_{4,1} = 60k$ based on the available data due to this shift.

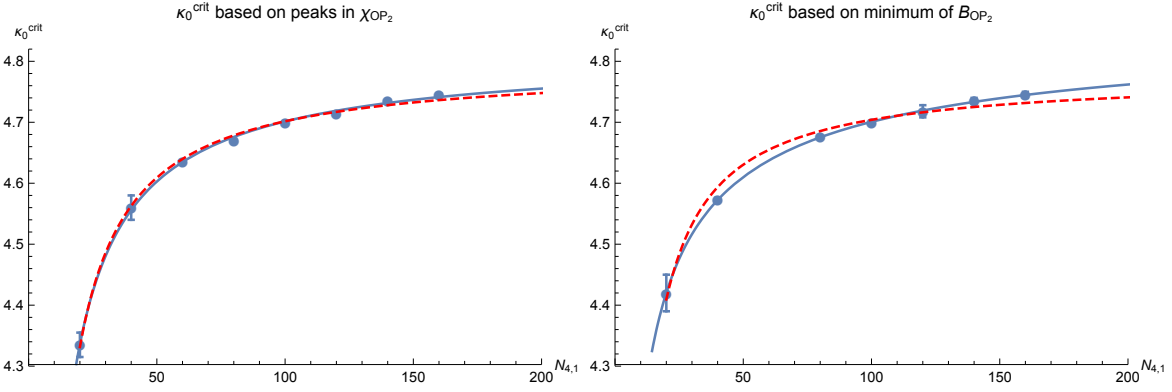


Figure 9: The left plot shows the lattice volume dependence of pseudo-critical points κ_0^{crit} as determined by locating the peak values of χ_{OP_2} for lattice volumes $N_{4,1} = 20k, 40k, 60k, 80k, 100k, 120k, 140k, 160k$ together with a fit to Eq. (4) (solid blue line) for which $\gamma = 1.16 \pm 0.07$ and the same fit with a forced value of $\gamma = 1$ (dashed red line). The right plot shows the lattice volume dependence of pseudo-critical points κ_0^{crit} as determined by locating the minimum of B_{OP_2} for lattice volumes $N_{4,1} = 20k, 40k, 80k, 100k, 120k, 140k, 160k$ together with a fit to Eq. (4) (solid blue line) for which $\gamma = 1.64 \pm 0.18$ and the same fit with a forced value of $\gamma = 1$ (dashed red line).

One can also measure the minimum (critical) value $B_{OP_2}^{min}$, defined by Eq. (6), as shown in Fig. 10. As the lattice volume increases the value of $B_{OP_2}^{min}$ moves away from zero, which bolsters the conclusion that the A - C transition is first order.

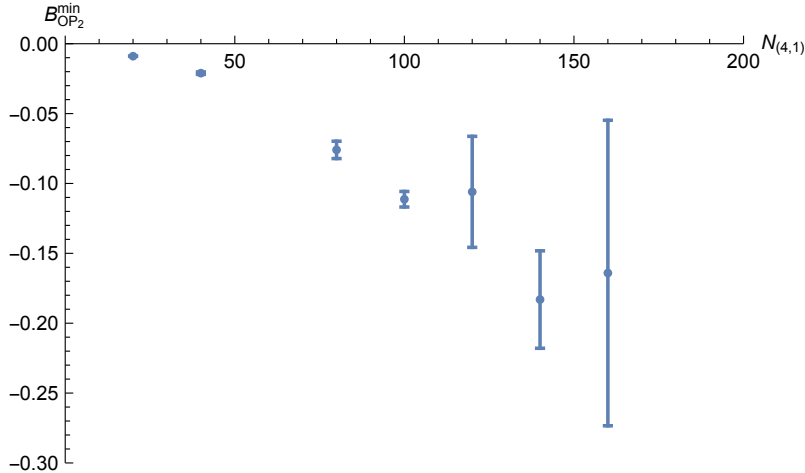


Figure 10: The dependence of the minimum of the Binder cumulant $B_{OP_2}^{min}$ as defined by Eqs. (5) and (6) on the system size $N_{4,1}$ for $\Delta = 0.6$.

3.2 Impact of the volume fixing method

In this section we keep the number of time slices fixed at $T = 80$ and investigate what impact, if any, the choice of fixing N_4 or $N_{4,1}$ has on critical phenomena at the A - C transition, and in particular whether double peaks are present in a histogram analysis using either volume fixing method.

3.2.1 Fixed $N_4 = 120k$ ($T = 80$)

Here, we successfully reproduce, albeit for a different order parameter, the result published in Ref. [17] for the A - C transition with $\kappa_0 = 4.710$, $\Delta = 0.6$ for fixed $N_4 = 120k$ and using $T = 80$ time slices, as shown in Figs. 11 and 12. As can be seen in Fig. 11 the Monte Carlo time history exhibits near-discontinuous jumps between two metastable states characterised by distinct values of $OP_2 \equiv N_{3,2}/N_{4,1}$, with the histogram of this data (Fig. 12) yielding a clear double peak structure.

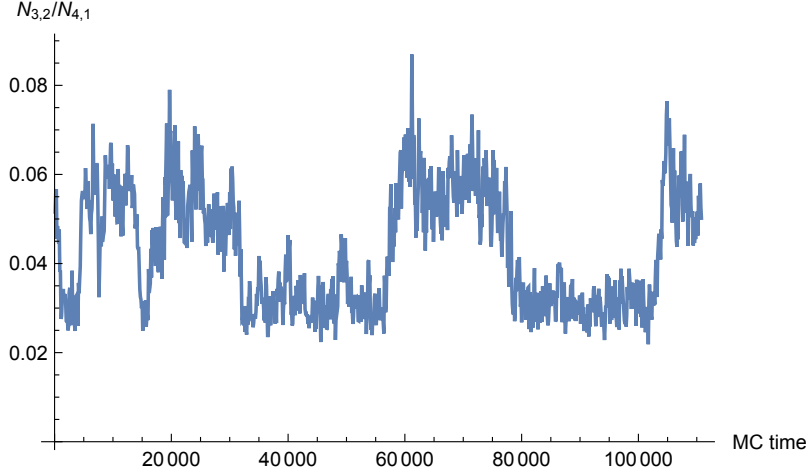


Figure 11: Monte Carlo time history of $OP_2 \equiv N_{3,2}/N_{4,1}$ at $\kappa_0 = 4.710$, $\Delta = 0.6$ for fixed $N_4 = 120k$ and with $T = 80$ time slices.

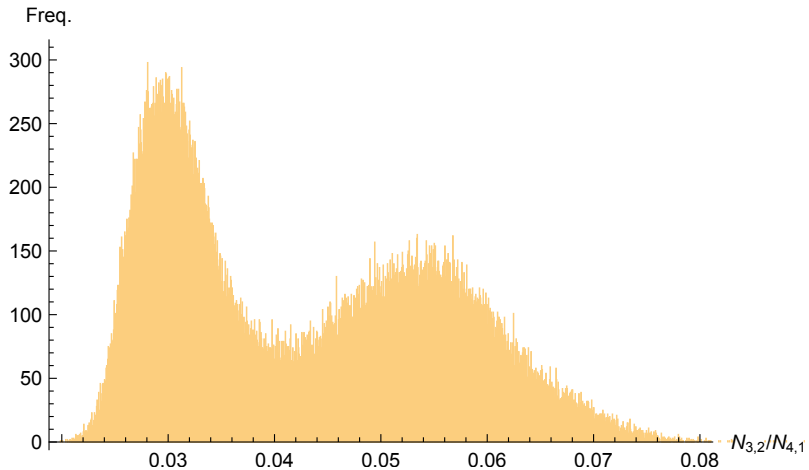


Figure 12: Histogram of $OP_2 \equiv N_{3,2}/N_{4,1}$ values at $\kappa_0 = 4.710$, $\Delta = 0.6$ for fixed $N_4 = 120k$ and with $T=80$ time slices.

3.2.2 Fixed $N_{4,1} = 115.2k$ ($T = 80$)

In order to make a more direct comparison between the two volume fixing methods we keep the bare couplings the same as in subsection 3.2.1, namely $\kappa_0 = 4.710$ and $\Delta = 0.6$. Reading off the value of $\overline{OP_2} \approx 0.04$ that is equidistant between the two Gaussian peaks in the histogram in Fig. 12, measured for $\overline{N_4} = 120,000$ and using

$$\overline{N_4} = \overline{N_{4,1}} + \overline{N_{3,2}} = \overline{N_{4,1}} (1 + \overline{OP_2}), \quad (15)$$

where the over-line denotes an average quantity, allows us to determine the average number of $N_{4,1}$ simplices to be $\overline{N_{4,1}} = 115,200$ at the transition point. We can therefore keep the same bare couplings as before but fix the number of $N_{4,1}$ simplices at $\overline{N_{4,1}} = 115.2k$. The results of this study are shown in Figs. 13 and 14, where it is clear that a double peak structure in the histogram is present for the exact same bare couplings when $N_{4,1}$ is fixed instead of N_4 . Thus, a double peak in the histogram of $OP_2 \equiv N_{3,2}/N_{4,1}$ is present at the transition point regardless of the particular volume fixing method.

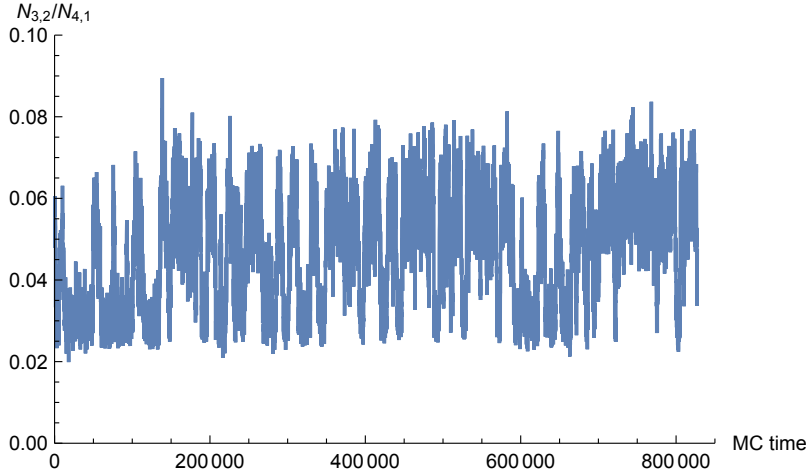


Figure 13: Monte Carlo time history of $OP_2 \equiv N_{3,2}/N_{4,1}$ at $\kappa_0 = 4.710$, $\Delta = 0.6$ for fixed $N_{4,1} = 115.2k$ and with $T = 80$ time slices.

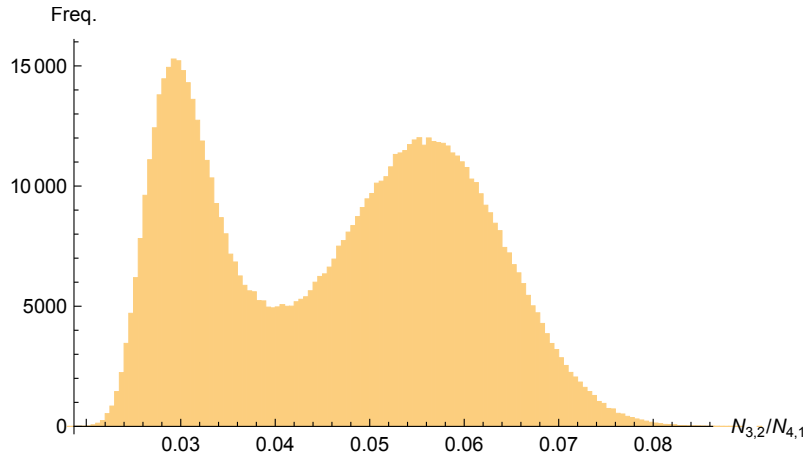


Figure 14: Histogram of $OP_2 \equiv N_{3,2}/N_{4,1}$ values at $\kappa_0 = 4.710$, $\Delta = 0.6$ for fixed $N_{4,1} = 115.2k$ and with $T=80$ time slices.

3.3 Impact of the time slicing

As demonstrated in subsection 3.2, the presence of a double peak structure in the histogram of $OP_2 \equiv N_{3,2}/N_{4,1}$ at the transition point does not seem to depend on the particular volume fixing

method. However, might it depend on the number of time slices used in the numerical simulations? In particular, limiting the number of time slices below a certain limit changes the semiclassical spatial volume profile of phase C from the de Sitter solution of a \cos^3 curve to a flat profile as, due to the limited number of time slices, the blob-like solution cannot form. Consequently, the phase transition no longer “breaks” the time-translation symmetry (in the sense described in footnote 7) when moving from phase A to phase C . This in principle may have an impact on the nature of the phase transition. To investigate the impact of limiting the CDT proper-time period we repeat the analysis of subsection 3.2 using $T = 4$ time slices.

3.3.1 Fixed $N_4 = 120k$ ($T = 4$)

Due to the different number of time slices one may expect a shift in the finite size effects, and so the transition point is expected to shift. Therefore, we must again locate the pseudo-critical κ_0^{crit} value by finding the peak of the susceptibility χ_{OP_2} as a function of κ_0 . As shown in Fig. 15, the peak of susceptibility of OP_2 is not pronounced but, as described in section 2, one can observe a clear peak in susceptibility of $\sqrt{OP_2}$ for $\kappa_0 \approx 4.825$. We then analyse the Monte Carlo time history of $OP_2 \equiv N_{3,2}/N_{4,1}$ in the form of histograms in the vicinity of this κ_0 value, as shown in Fig. 16. No double peak structure in the histogram of OP_2 is observed up to a resolution of three decimal places in κ_0 . However, at $\kappa_0 = 4.825$ the value of OP_2 evolves entirely within one metastable state and at $\kappa_0 = 4.826$ within a distinctly different state (see Fig. 16 for the histograms of this data), and so presumably somewhere within the range $\kappa_0 = 4.825 - 4.826$ lies the true pseudo-critical κ_0^{crit} value, although this is yet to be established.

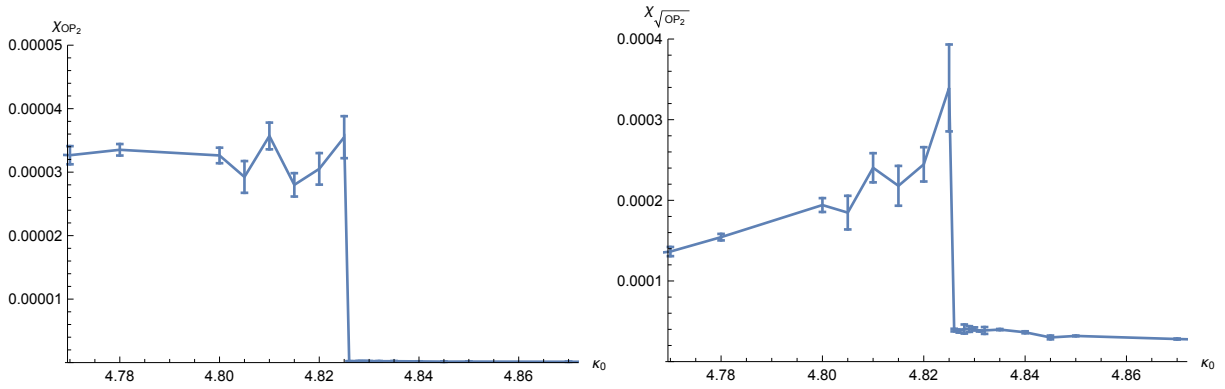


Figure 15: The susceptibility χ_{OP_2} as defined by Eq. (3) (left chart) and the susceptibility $\chi_{\sqrt{OP_2}}$ (right chart) as a function of κ_0 for fixed $N_4 = 120k$ with $T = 4$ time slices.

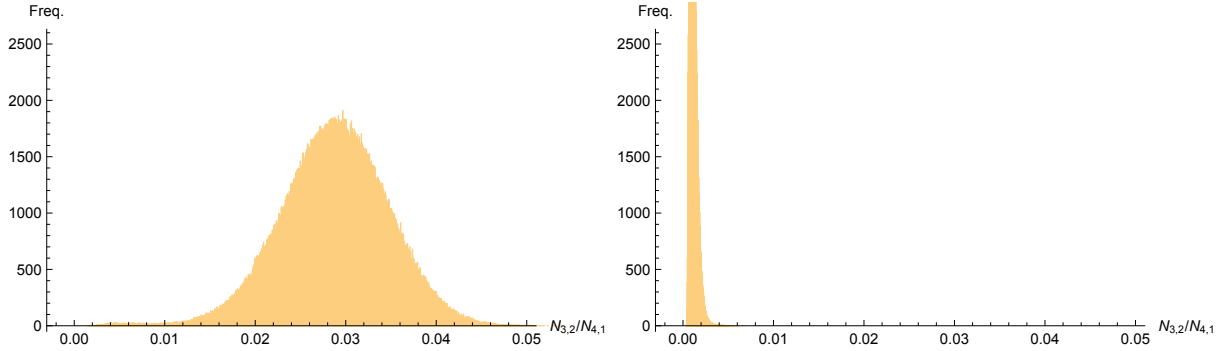


Figure 16: Histogram of $OP_2 \equiv N_{3,2}/N_{4,1}$ values at $\kappa_0 = 4.825$, $\Delta = 0.6$ (left) and $\kappa_0 = 4.826$, $\Delta = 0.6$ (right) for fixed $N_4 = 120k$ and with $T = 4$ time slices.

3.3.2 Fixed $N_{4,1} = 115.2k$ ($T = 4$)

The pseudo-critical κ_0 value is again determined by locating the peak value of the susceptibility χ_{OP_2} or (like in section 3.3.1) $\chi_{\sqrt{OP_2}}$ as a function of κ_0 , as shown in Fig. 17. Again, such an analysis indicates the κ_0^{crit} value is likely in the range $\kappa_0^{crit} = 4.828 - 4.829$, however no double peak structure in the histogram of the Monte Carlo time history of OP_2 is observed up to a resolution of three decimal places in κ_0 . However, at $\kappa_0 = 4.828$ the value of OP_2 evolves entirely within one metastable state and at $\kappa_0 = 4.829$ within a distinctly different state (see Fig. 18 for the histograms of this data), and so presumably somewhere within the range $\kappa_0 = 4.828 - 4.829$ lies the true pseudo-critical κ_0 value, although this is yet to be established.

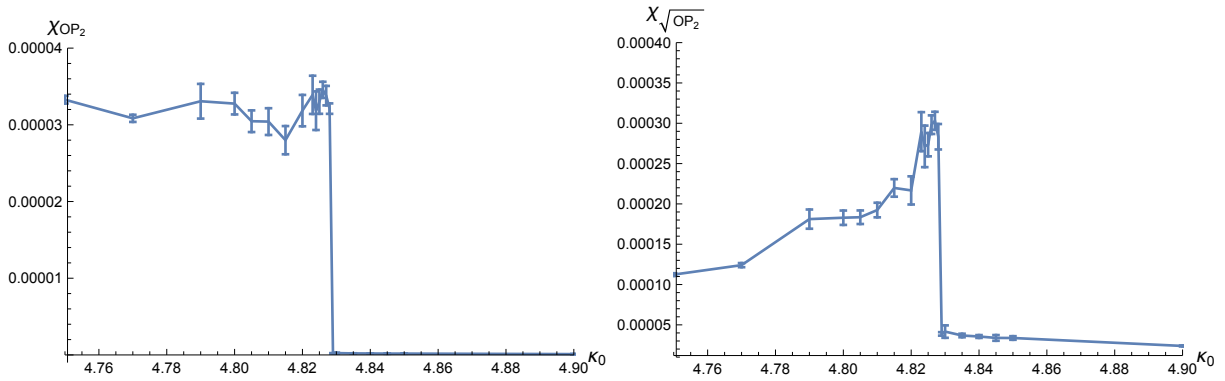


Figure 17: The susceptibility χ_{OP_2} as defined by Eq. (3) (left chart) and the susceptibility $\chi_{\sqrt{OP_2}}$ (right chart) as a function of κ_0 for fixed $N_{4,1} = 115.2k$ with $T = 4$ time slices.

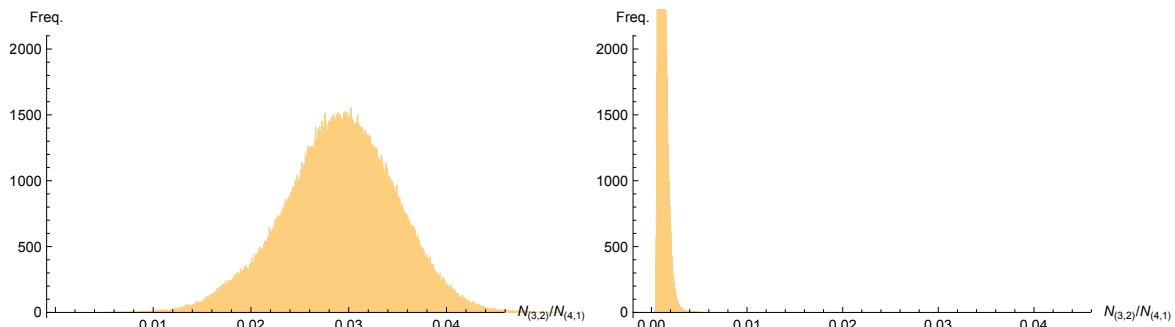


Figure 18: Histogram of $OP_2 \equiv N_{3,2}/N_{4,1}$ values at $\kappa_0 = 4.828$, $\Delta = 0.6$ (left) and $\kappa_0 = 4.829$, $\Delta = 0.6$ (right) for fixed $N_{4,1} = 115.2k$ and with $T = 4$ time slices.

3.4 Summary for the spherical topology case.

Summing up this part, using the $OP_2 \equiv N_{3,2}/N_{4,1}$ order parameter we have analysed in detail the $A-C$ transition for a system with spherical spatial topology, $T = 80$ time slices and $N_{4,1}$ volume fixing. We have confirmed all signatures of the first order transition, i.e. the OP_2 histograms showing double peak structure at the transition points, the scaling exponent of $\gamma \approx 1$ and the divergence of $B_{OP_2}^{min}$ from zero when the lattice volume is increased, as earlier reported in Ref. [17] for the system with N_4 volume fixed and the N_0 order parameter. We then checked the impact of the volume fixing method and the number of time slices on our results. We have focused on the existence of the double peak structure in the histograms of OP_2 measured at the transition points and we have skipped the detailed discussion of the transition point position and the Binder cumulant scaling with lattice volume. The reason is two-fold. Firstly, phase transition studies are very time consuming and thus we were not able to repeat the numerical simulations for all 8 system sizes described in section 3.1 for all the cases discussed herein, but we focused on gaining large statistics in only a few (big size) systems. Secondly, the $A-C$ transition with the N_4 volume fixed was already analysed in detail in Ref. [17], albeit for a different order parameter N_0 , but we believe that all the previous results concerning finite size scaling become valid also for the OP_2 when the N_4 volume is fixed. This is corroborated by our measurements of the histogram of the OP_2 which behaves exactly the same way as the N_0 parameter described in Ref. [17]. All the results for the $T = 80$ time slices show a double peak structure in the histogram of OP_2 measured at the transition points, which provides strong evidence that the transition is first order independent of the volume fixing method. The ambiguous results come from measurements with $T = 4$ time slices (see section 3.3). In this case, we can not confirm a double peak structure in the histograms up to a resolution of three decimal places in κ_0 . However, an analysis of the Monte Carlo time evolution either side of the putative transition suggests a double peak structure is likely to emerge for a greater resolution of κ_0 . This is probably a consequence of finite size effects being different for the $T = 4$ systems compared to the $T = 80$ triangulations, where the effective volume per slice is much lower. As a result, the separation of the metastable states is much more pronounced in the $T = 4$ systems making the transition much sharper. Such a behaviour corroborates the first order nature of the $A - C$ transition.

4 Toroidal topology

4.1 The order of the A - C transition

We will now study the impact of topology change on the properties of the A - C transition. We will focus on systems with toroidal topology of spatial slices, which we started to investigate some time ago (for details see Refs. [23, 24, 9, 22]). We start our discussion from a system with $T = 4$ time slices and with $N_{4,1}$ volume fixing. The reason for this choice is two-fold. Firstly, the systems with such parameters were earlier used to explore the toroidal CDT phase diagram presented in Ref. [22], where it was noted that the order parameters change smoothly between the A and C phases and one does not observe any separation of states, nor any double peak structure on the OP histograms at the transition points. Such a behaviour may suggest that the A - C transition is now higher order. Therefore we want to check this in detail by performing a proper finite-size scaling analysis. Secondly, as noted in Ref. [23], it seems that due to a much larger minimal triangulation the finite size effects are bigger in toroidal CDT compared to spherical CDT and thus in the former case one should use systems with a much larger spatial volume for single time slices, which is obtained for small T . We will then investigate the impact that both time slicing and volume fixing has on our results.

We again focus on the OP_2 parameter as defined by Eq.(14). Measurements presented in this section were made for the same choice of $\Delta = 0.6$ as for the spherical topology case, discussed in section 3. We analysed systems with $T = 4$ time slices for 11 different lattice volumes¹⁰: $N_{4,1} = 20k, 40k, 60k, 80k, 100k, 120k, 160k, 200k, 300k, 400k$ and $500k$. In order to ensure a proper thermalization of our data, and to estimate the accuracy of our measurements, as well as to check possible hysteresis effects we performed two independent runs for each Monte Carlo simulation, one initiated with a configuration from phase A and another one with a configuration from phase C . After thermalizing both runs should converge and give (statistically) similar results. Data collected during the thermalization period is not included in our final measurements.

As already discussed in Section 2, for toroidal topology one cannot observe the susceptibility peaks when using OP_2 , but they can be observed when using $\sqrt{OP_2}$, thus in the following we will focus on this latter function. We again start by locating the pseudo critical κ_0^{crit} values by finding maxima in the susceptibility $\chi_{\sqrt{OP_2}} \approx \frac{\chi_{OP_2}}{\langle OP_2 \rangle}$ as a function of κ_0 (see Fig. 19) separately for each lattice volume.

¹⁰The results for the Binder cumulant were obtained only for 8 lattice volumes: $N_{4,1} = 20k, 40k, 60k, 100k, 200k, 300k, 400k$ and $500k$.

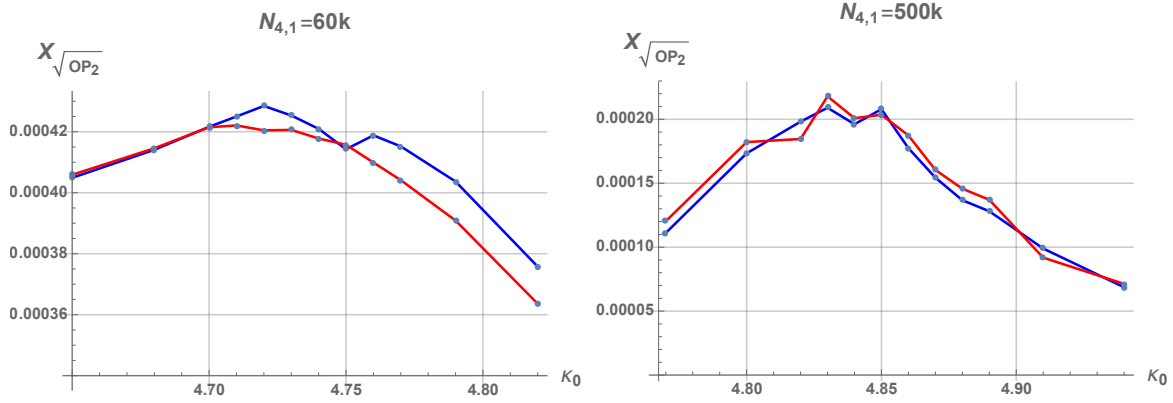


Figure 19: The susceptibility $\chi_{\sqrt{OP_2}} \approx \frac{\chi_{OP_2}}{\langle OP_2 \rangle}$ as defined by Eqs. (3) and (8) as a function of κ_0 for $N_{4,1} = 60k$ (left) and $N_{4,1} = 500k$ (right). The blue line corresponds to simulations initiated deep in phase A and the red line to simulations initiated deep in phase C.

One can see that the peaks in Fig. 19 are relatively flat and despite the long simulation time¹¹ there is still a small discrepancy between data measured using the two alternative starting configurations, yielding relatively large error bars for the position of the pseudo-critical κ_0^{crit} values, as shown in Figure 20. The position of the susceptibility peaks and the resulting position of the pseudo-critical points at which the transition occurs shows a strong volume dependence. One can again use the finite-size scaling relation of equation (4) to fit the critical exponent γ to the measured $\kappa_0^{crit}(N_{4,1})$ data (see Fig. 20). The best fit yields a shift exponent of $\gamma = 1.22 \pm 0.08$ which is slightly higher than the γ value measured for the spherical case (see section 3.1), but still consistent with $\gamma = 1$ of a first order transition.

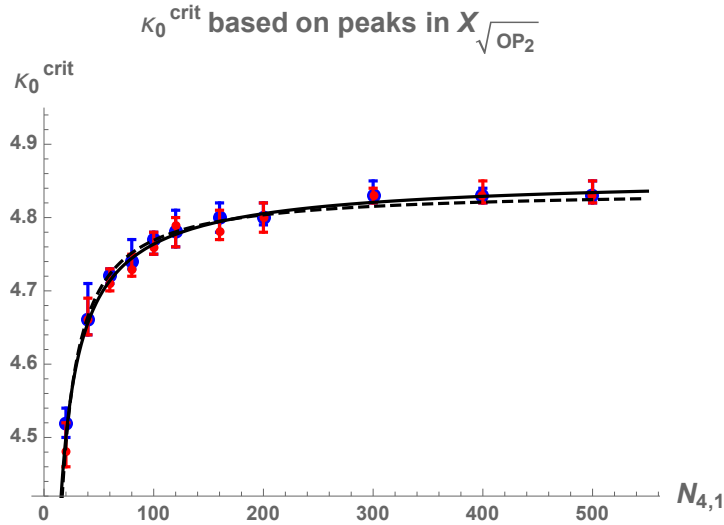


Figure 20: Lattice volume dependence of pseudo-critical points κ_0^{crit} based on the position of susceptibility $\chi_{\sqrt{OP_2}}$ peaks measured for 11 different lattice volumes $N_{4,1} = 20k, 40k, 60k, 80k, 100k, 120k, 160k, 200k, 300k, 400k, 500k$ together with a fit to Eq. (4) (solid line) for which $\gamma = 1.22 \pm 0.08$ and the same fit with a forced value of $\gamma = 1$ (dashed line). The blue data are for simulations initiated deep in phase A and the red data for simulations initiated deep in phase C.

¹¹The Monte Carlo simulations described in this section had around 5×10^{12} attempted MC moves each and they took almost half a year to complete.

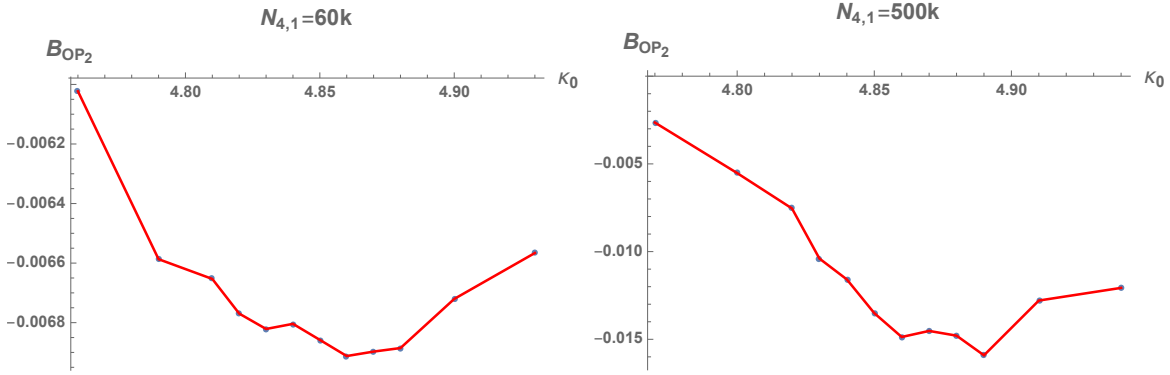


Figure 21: The Binder cumulant $B_{OP_2} \approx B_{\sqrt{OP_2}} \approx -\chi_{\ln OP_2}$ as defined by Eqs. (5) (and Eqs. (10), (12)) as a function of κ_0 for $N_{4,1} = 60k$ (left) and $N_{4,1} = 500k$ (right).

One can repeat the above finite size analysis, now looking at minima (see Fig. 21) of the Binder cumulant of OP_2 defined in Eq. (5).¹² The Binder cumulant (as a function of κ_0) was measured for 8 different lattice volumes: $N_{4,1} = 20k, 40k, 60k, 100k, 200k, 300k, 400k$ and $500k$. The pseudo-critical κ_0^{crit} values located this way are shifted towards a higher κ_0 from the values measured by the location of susceptibility peaks, discussed above. This kind of discrepancy is possible as positions of the Binder cumulant minima are expected to show smaller finite size dependence than the positions of the susceptibility maxima. This is indeed the case as illustrated in Fig. 22, where we plot the lattice volume dependence of κ_0^{crit} values based on the Binder cumulant minima.

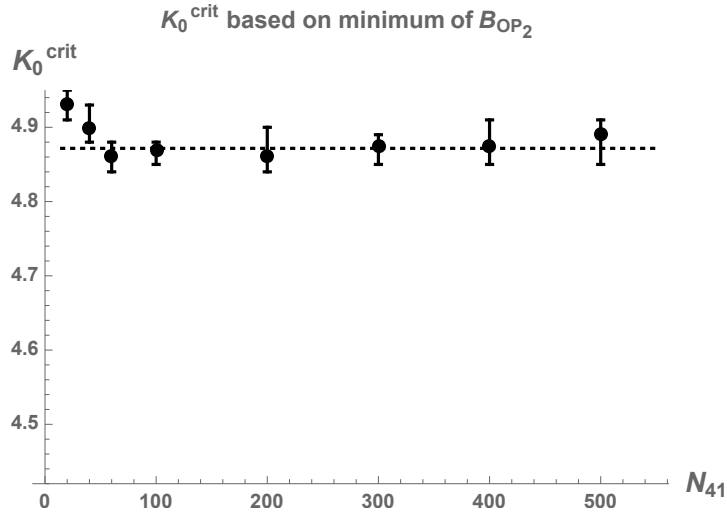


Figure 22: Lattice volume dependence of pseudo-critical points κ_0^{crit} based on the position of the Binder cumulant B_{OP_2} minima measured for 8 different lattice volumes $N_{4,1} = 20k, 40k, 60k, 100k, 200k, 300k, 400k, 500k$ together with an estimate of the true critical value of $\kappa_0^{crit}(\infty) = 4.87 \pm 0.01$ (dotted line).

In Fig.22 we keep the same range of the vertical axis as in Fig. 20 so that it is clearly visible that the pseudo-critical value κ_0^{crit} is now (almost) volume independent. This may suggest that, due to smaller finite size effects when using the Binder cumulants, one has reached the system

¹²As discussed in section 2, it is also consistent with the Binder cumulant of $\sqrt{OP_2}$ and with the susceptibility of $\ln OP_2$ (see Eqs. (10) and (12)): $B_{OP_2} \approx B_{\sqrt{OP_2}} \approx -\chi_{\ln OP_2}$.

size at which the measured pseudo-critical $\kappa_0^{crit}(N_{4,1})$ values are very close to the true critical $\kappa_0^{crit}(\infty)$ value in the infinite volume limit. By taking the mean value of $\kappa_0^{crit}(N_{4,1})$ measured for $N_{4,1} \geq 60k$ ¹³ one can estimate the true critical value to be $\kappa_0^{crit}(\infty) = 4.87 \pm 0.01$. One can then use this estimate to refit the pseudo-critical $\kappa_0^{crit}(N_{4,1})$ values, measured using the susceptibility peaks method, to the finite-size scaling relation (4), now with forced value of $\kappa_0^{crit}(\infty) = 4.87$. This way one obtains a slightly corrected estimate of the critical exponent of $\gamma = 1.31 \pm 0.03$. One should note that the above accuracy of the γ exponent is just the fit error and it does not take into account statistical errors of the data points. The result is now less consistent with $\gamma = 1$ expected from a first order transition, but, as presented in Figure 23, the critical exponent of $\gamma = 1$ cannot be excluded within the error bars of the measured κ_0^{crit} data points.

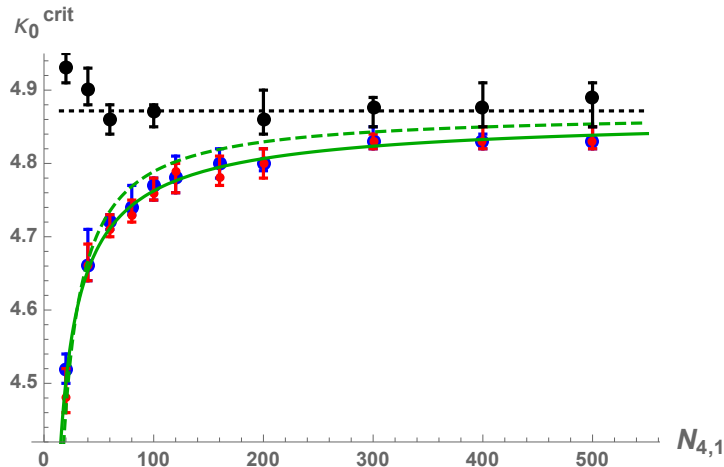


Figure 23: Lattice volume dependence of pseudo-critical points κ_0^{crit} based on the susceptibility maxima (blue and red data points) and on the Binder cumulant minima (black data points). The estimate of the true critical value of $\kappa_0^{crit}(\infty) = 4.87 \pm 0.01$ is presented as a black dotted line. The fit to Eq. (4) with forced $\kappa_0^{crit}(\infty) = 4.87$ for which $\gamma = 1.31 \pm 0.03$ is drawn as a green solid line and the same fit with a forced value of $\gamma = 1$ as a green dashed line.

The Binder cumulant data of the OP_2 parameter, discussed above, can also be used to check how the minimal (critical) value $B_{OP_2}^{min}$, defined by Eq. (6), depends on $N_{4,1}$. As shown in Fig. 24, the value of $B_{OP_2}^{min}$ moves away from zero when the lattice volume is increased. Although the scaling of $B_{OP_2}^{min}$ as a function of $N_{4,1}$ seems to be power-like, it is quite unlikely that this kind of behaviour can persist in the infinite volume limit. Anyway, the observed divergence from zero with increased lattice volume is expected for a first order transition and it is usually attributed to the existence of two metastable states at the transition point.

¹³We have excluded the first two data points, for $N_{4,1} = 20k$ and $40k$, from the mean as they still show a small volume dependency - see Fig. 22.

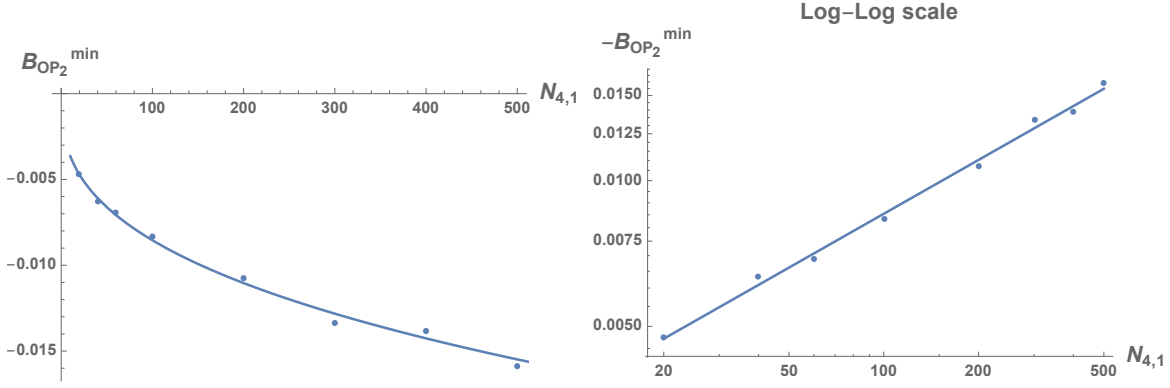


Figure 24: The dependence of (the minimum of) the Binder cumulant $B_{OP_2}^{min}$ as defined by Eqs. (5) and (6) on the system size $N_{4,1}$ at the A - C transition for $\Delta = 0.6$. The log-log plot on the right shows a clear powerlaw behaviour.

Therefore, we have finally performed a very careful Monte Carlo time history analysis for all our data in search of the double peak structure in the measured OP_2 histograms. In agreement with preliminary findings of Ref. [22], we could not observe neither metastable state jumping nor double peaks of the OP_2 parameter nor its functions¹⁴ at any of the transition points - all measured histograms have a Gaussian-like shape with only one peak, as presented in Fig. 25. As the position of the pseudo-critical points κ_0^{crit} is different for the susceptibility and for the Binder cumulant observables we have also analysed the histograms for all other measured κ_0 data points, but in each case a single Gaussian peak was present.

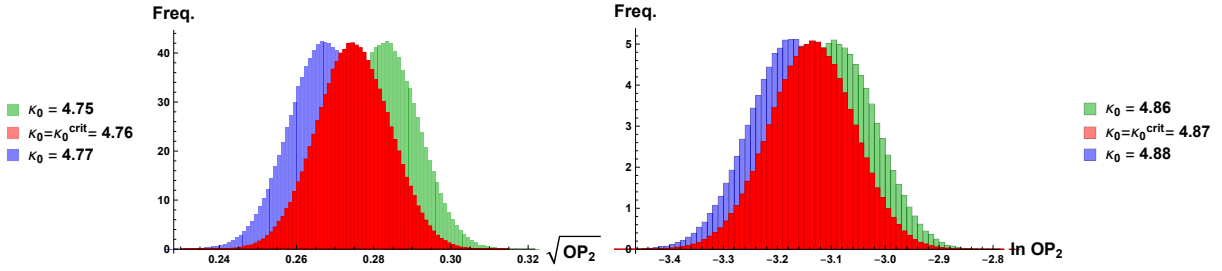


Figure 25: Exemplary histograms of the (functions of) order parameter $OP_2 \equiv N_{3,2}/N_{4,1}$ at pseudo-critical κ_0^{crit} values for $\Delta = 0.6$ with fixed lattice volumes $N_{4,1} = 100k$. The left chart presents the histograms of $\sqrt{OP_2}$ measured in the vicinity of $\kappa_0^{crit} = 4.76$ based on the position of the susceptibility $\chi_{\sqrt{OP_2}}$ peak, and the right chart shows the histograms of $\ln OP_2$ measured in the vicinity of $\kappa_0^{crit} = 4.87$ based on the position of the Binder cumulant B_{OP_2} minimum. The histograms plotted in red are exactly at the transition points, while the green / blue data are for histograms measured for slightly lower / higher value of κ_0 than the critical value. The red, green and blue histograms overlap showing that the transition is smooth, allowing no space for the existence of any more than one state at the transition point.

To conclude this part, although we did not observe any metastable state jumping of the order parameter (all the OP_2 histograms had just a single peak with a Gaussian-like shape), both the value of the critical shift exponent γ (which is close to one) and scaling of the Binder cumulant $B_{OP_2}^{min}$ with the lattice volume ($B_{OP_2}^{min}$ diverges from zero) suggest that the A - C transition remains

¹⁴As we have located the pseudo-critical κ_0^{crit} values by using either the susceptibility $\chi_{\sqrt{OP_2}}$ or the Binder cumulant $B_{OP_2} \approx -\chi_{\ln OP_2}$ we have also checked the histograms of $\sqrt{OP_2}$ in the former and of $\ln OP_2$ in the later case, respectively.

first order in the case of toroidal topology. The transition is not as sharp as in the spherical case, which may be attributed to much larger finite size effects in toroidal CDT compared with spherical CDT.

4.2 Impact of the time slicing

In this section we will investigate what impact, if any, the choice of the number of time slices used in the MC numerical simulations has on critical phenomena at the A - C transition, now in the toroidal CDT case. We keep the volume fixing method of Section 4.1, i.e. the total number of $(4, 1)$ simplices is fixed at $N_{4,1} = 200k$ and we change the number of time slices to $T = 10, 20, 40$.

We start by investigating the scaling properties of the order parameter $OP_2 \equiv N_{4,1}/N_{3,2}$ measured at the vicinity of the A - C transition. In particular, we want to check the scaling of the mean value $\langle OP_2 \rangle$ and the susceptibility χ_{OP_2} with T when the average spatial volume $\langle n_t \rangle = N_{4,1}/T$ is kept fixed. By using approximations (8), (9) (10) and (12) these scaling relations will automatically translate into scaling of $\chi_{\sqrt{OP_2}} \approx \frac{\chi_{OP_2}}{\langle OP_2 \rangle}$ and $B_{OP_2} \approx -\frac{\chi_{OP_2}}{\langle OP_2 \rangle^2}$.

In the toroidal CDT case, as opposed to the spherical case, the average volume profile does not change between phase A and phase C where in both phases $\langle n_t \rangle = N_{4,1}/T = \text{const.}$ We therefore suspect that the order parameter and its fluctuations depend on $\langle n_t \rangle$. As demonstrated in Fig. 26, the mean $\langle OP_2 \rangle$ does not depend on T when $\langle n_t \rangle$ is kept fixed, however it is different for each value of $\langle n_t \rangle = \text{const.}$ The OP_2 fluctuations, measured by the susceptibility $\chi_{OP_2} \equiv \langle OP_2^2 \rangle - \langle OP_2 \rangle^2$, scale (approximately) as $1/T$ when $\langle n_t \rangle$ is kept fixed. This is shown in Fig. 27. This kind of scaling may suggest that, in the vicinity of the A - C transition, the OP_2 can be modelled by T statistically independent identical random variables indexed by $t = 1, \dots, T$. In such a case one has $OP_2 = \frac{1}{T} \sum_t \widetilde{OP}_2(n_t)$, where $\widetilde{OP}_2(n_t)$ denotes the value of the order parameter in each time slice, which depends solely on n_t . Consequently

$$\langle OP_2 \rangle = \left\langle \frac{1}{T} \sum_t \widetilde{OP}_2(n_t) \right\rangle = \left\langle \widetilde{OP}_2(N_{4,1}/T) \right\rangle, \quad (16)$$

$$\chi_{OP_2} = \chi_{\frac{1}{T} \sum_t \widetilde{OP}_2(n_t)} = \frac{\chi_{\widetilde{OP}_2(N_{4,1}/T)}}{T}, \quad (17)$$

in accordance with the scaling observed for various choices of $N_{4,1}$ and T such that $\langle n_t \rangle = N_{4,1}/T$ is kept fixed, see Fig. 26 and 27.

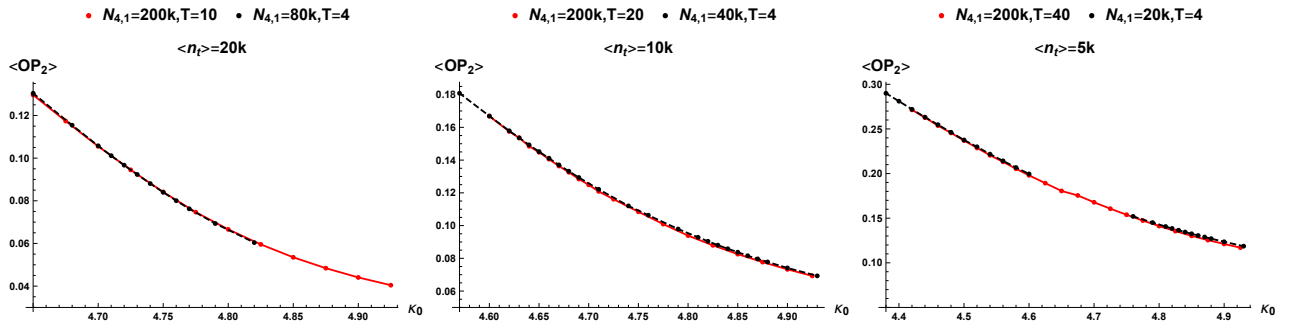


Figure 26: Mean value of the order parameter $\langle OP_2 \rangle$ as a function of κ_0 (red line) measured for fixed $N_{4,1} = 200k$ and $T = 10$ (left), $T = 20$ (middle) and $T = 40$ (right) compared to data measured for fixed $T = 4$ time slices (black-dashed line) and $N_{4,1} = 80k$ (left), $N_{4,1} = 40k$ (middle) and $N_{4,1} = 20k$ (right), respectively.

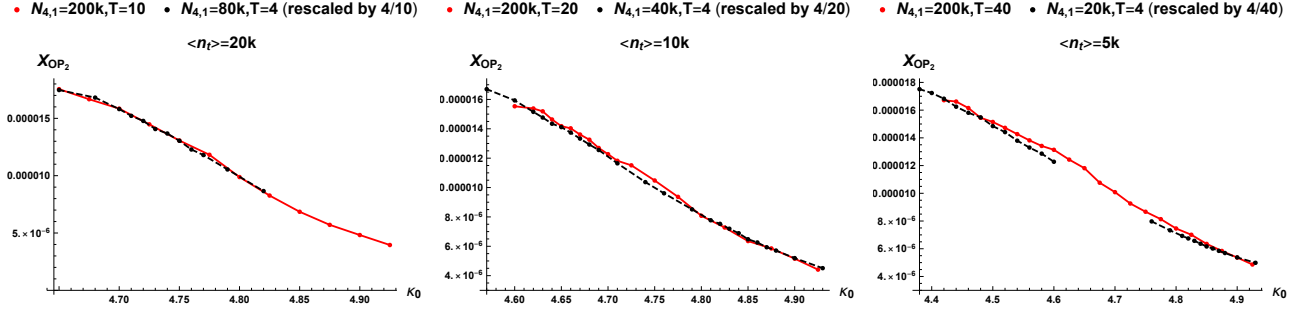


Figure 27: The susceptibility χ_{OP_2} as defined by Eq. (3) as a function of κ_0 (red line) measured for fixed $N_{4,1} = 200k$ and $T = 10$ (left), $T = 20$ (middle) and $T = 40$ (right) compared to rescaled data measured for fixed $T = 4$ time slices (black-dashed line) and $N_{4,1} = 80k$ (left), $N_{4,1} = 40k$ (middle) and $N_{4,1} = 20k$ (right), respectively.

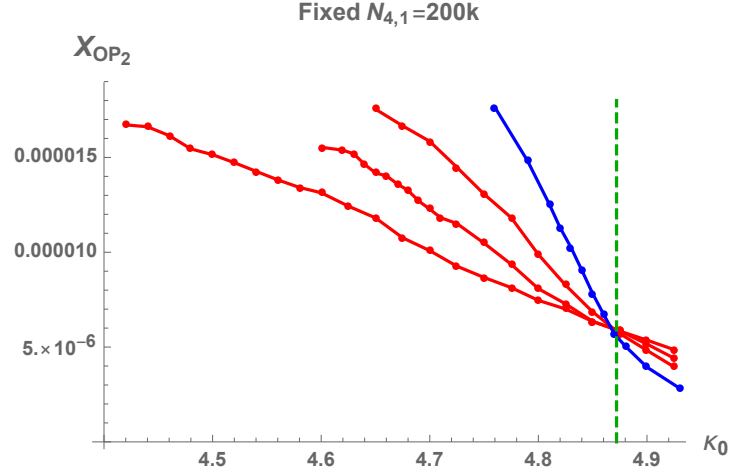


Figure 28: The susceptibility χ_{OP_2} as a function of κ_0 measured for fixed $N_{4,1} = 200k$ and various $T = 4$ (blue line) and $T = 10, 20, 40$ (red lines) and thus various $\langle n_t \rangle = N_{4,1}/T = 50k, 20k, 10k, 5k$, respectively. The curves cross at the $\kappa_0^{crit}(\infty) = 4.87$ point whose position is denoted by a green-dashed line.

What is more interesting is the following: for fixed $N_{4,1}$ the OP_2 fluctuations expressed by χ_{OP_2} as a function of κ_0 depend on $\langle n_t \rangle = N_{4,1}/T$, see Fig. 28, *but they seem to be universal at the true (infinite volume) transition point* $\kappa_0^{crit}(\infty) = 4.87$ (see Section 4.1). This is seen in Fig. 29 where the curves plotted for various $\langle n_t \rangle = N_{4,1}/T$ cross. Therefore, for fixed $N_{4,1}$, the true critical susceptibility $\chi_{OP_2}^{crit} \equiv \chi_{OP_2}(\kappa_0^{crit}(\infty))$ does not depend on T , which, in conjunction with relation (17), implies a universal critical scaling

$$\chi_{OP_2}^{crit} = \frac{\chi^*}{N_{4,1}}, \quad \chi^* = const., \quad (18)$$

valid for any $N_{4,1}$ and T . This is indeed the case, as illustrated in Fig. 29, where we plot $\chi_{OP_2} \cdot N_{4,1}$ as a function of κ_0 measured for various choices of both $N_{4,1}$ and T . In accordance with relation (18) all the curves cross at a single critical point $\kappa_0^{crit}(\infty) = 4.87$ resulting in a universal value of $\chi^* \approx 1.2$.

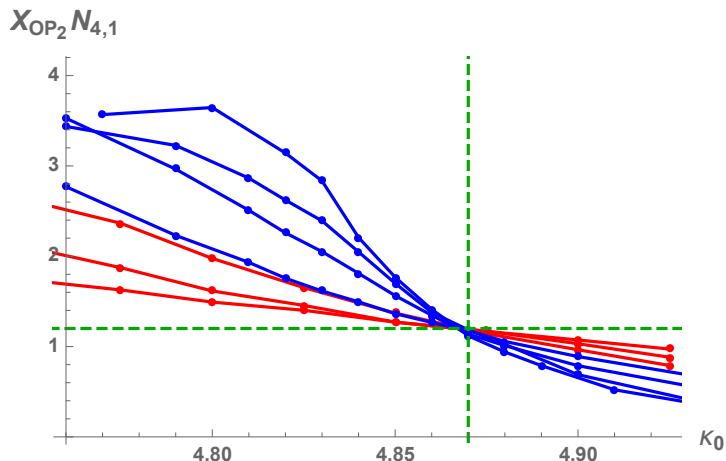


Figure 29: The (rescaled) susceptibility $\chi_{OP_2} \cdot N_{4,1}$ as a function of κ_0 measured for $N_{4,1} = 200k$ and $T = 10, 20, 40$ (red lines) and for $T = 4$ and $N_{4,1} = 100, 200, 300, 400$ (blue lines). All the curves cross at a single $(\kappa_0^{crit}(\infty); \chi^*) \approx (4.87; 1.2)$ point whose position is denoted by green-dashed lines.

All the above results show that data measured in numerical MC simulations with the $N_{4,1}$ volume fixed for various number of time slices T and various lattice volumes $N_{4,1}$ can be simply rescaled, resulting in universal critical behaviour of Eq. (18), and consistent with $\kappa_0^{crit}(\infty) = 4.87$ computed in Section 4.1. The critical scaling (18) of susceptibility of $OP_2 \equiv N_{3,2}/N_{4,1}$, which is an intensive parameter, automatically translates into the following scaling of susceptibility of the extensive parameter $N_{3,2}$:

$$\chi_{N_{3,2}}^{crit} = \chi^* \cdot N_{4,1}, \quad \chi^* = const., \quad (19)$$

which is typical for a first order transition. Thus the result strongly supports the first order nature of the $A - C$ transition in the toroidal topology.

We have also performed the histogram analysis of the OP_2 parameter at the transition points measured for fixed $N_{4,1} = 200k$ and various $T = 10$ (Fig. 32), $T = 20$ (Fig. 35) and $T = 40$ (Fig. 38). As in Section 4.1, in each case we have located the pseudo-critical κ_0^{crit} values by either looking at the susceptibility $\chi_{\sqrt{OP_2}}$ maxima or the Binder cumulant B_{OP_2} minima (see Fig. 30, Fig. 33 and Fig. 36, respectively), and we have measured the OP_2 Monte Carlo history at these points (see Fig. 31, Fig. 34 and Fig. 37, respectively). In each case, and also for any other κ_0 data point measured, the OP_2 order parameter (and its functions) shows Gaussian-like fluctuations and there are no signs of the metastable states jumping in any case. Again, this behaviour is not typical for a first order transition, but most likely, due to much larger finite size effects in the toroidal topology, we have not yet reached the lattice size where two distinct metastable states can be observed.

4.2.1 Fixed $N_{4,1} = 200k$ ($T = 10$)

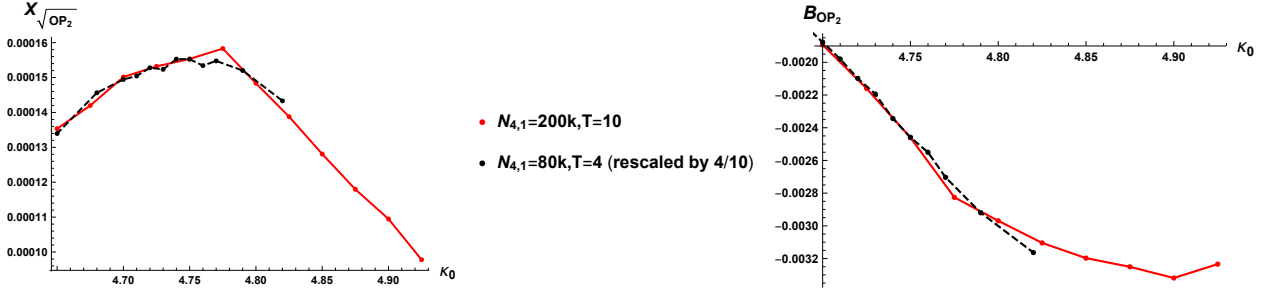


Figure 30: The susceptibility $\chi_{\sqrt{OP_2}} \approx \frac{\chi_{OP_2}}{\langle OP_2 \rangle}$ as defined by Eq. (3) (left chart) and the Binder cumulant B_{OP_2} as defined by Eq. (5) (right chart) as a function of κ_0 measured for fixed $N_{4,1} = 200k$ and $T = 10$ time slices (red line) and rescaled data for fixed $N_{4,1} = 80k$ and $T = 4$ time slices (black-dashed line).

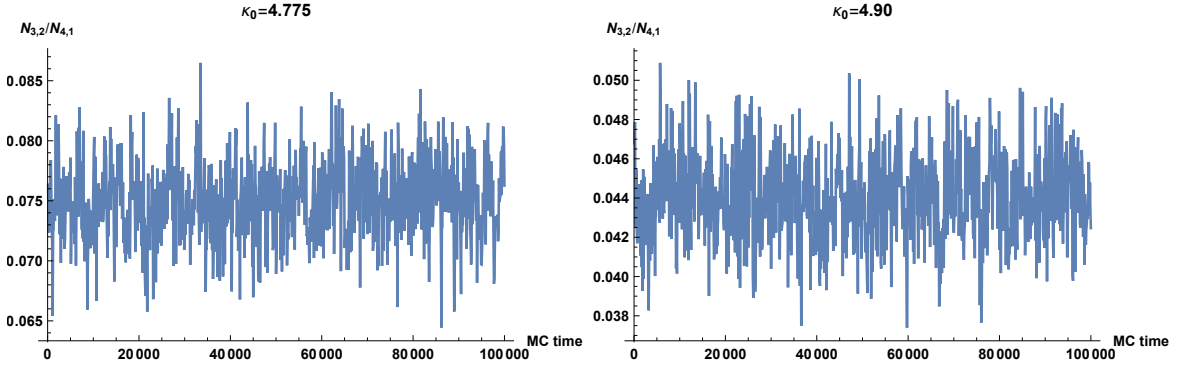


Figure 31: Monte Carlo time history of $OP_2 \equiv N_{3,2}/N_{4,1}$ at pseudo-critical points measured using the susceptibility method: $\kappa_0 = 4.775$ (left chart) and using the Binder cumulant method: $\kappa_0 = 4.90$ (right chart) for fixed $N_{4,1} = 200k$ and $T = 10$ time slices.

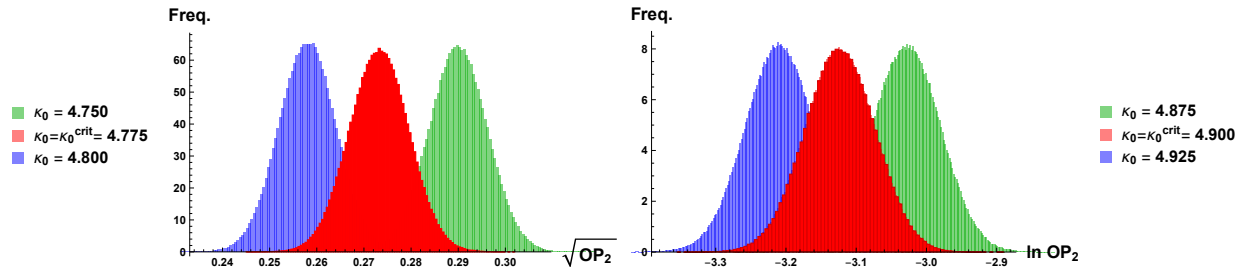


Figure 32: Exemplary histograms of the (functions of) order parameter $OP_2 \equiv N_{3,2}/N_{4,1}$ at pseudo-critical κ_0^{crit} values with fixed $N_{4,1} = 200k$ and $T = 10$ time slices. The left chart presents the histograms of $\sqrt{OP_2}$ measured in the vicinity of $\kappa_0^{crit} = 4.775$ based on the position of the susceptibility $\chi_{\sqrt{OP_2}}$ peak (Fig. 30, left), and the right chart shows the histograms of $\ln OP_2$ measured in the vicinity of $\kappa_0^{crit} = 4.90$ based on the position of the Binder cumulant B_{OP_2} minimum (Fig. 30, right). The histograms plotted in red are exactly at the transition points, while the green / blue data are for histograms measured for slightly lower / higher value of κ_0 than the critical value. The red, green and blue histograms overlap showing that the transition is smooth, allowing no space for the existence of any more than one state at the transition point.

4.2.2 Fixed $N_{4,1} = 200k$ ($T = 20$)

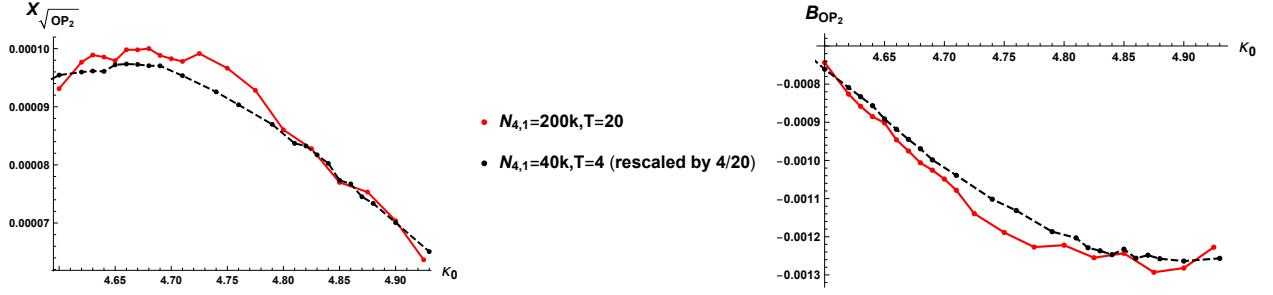


Figure 33: The susceptibility $\chi_{\sqrt{OP_2}} \approx \frac{\chi_{OP_2}}{\langle OP_2 \rangle}$ as defined by Eq. (3) (left chart) and the Binder cumulant B_{OP_2} as defined by Eq. (5) (right chart) as a function of κ_0 measured for fixed $N_{4,1} = 200k$ and $T = 20$ time slices (red line) and rescaled data for fixed $N_{4,1} = 40k$ and $T = 4$ time slices (black-dashed line).

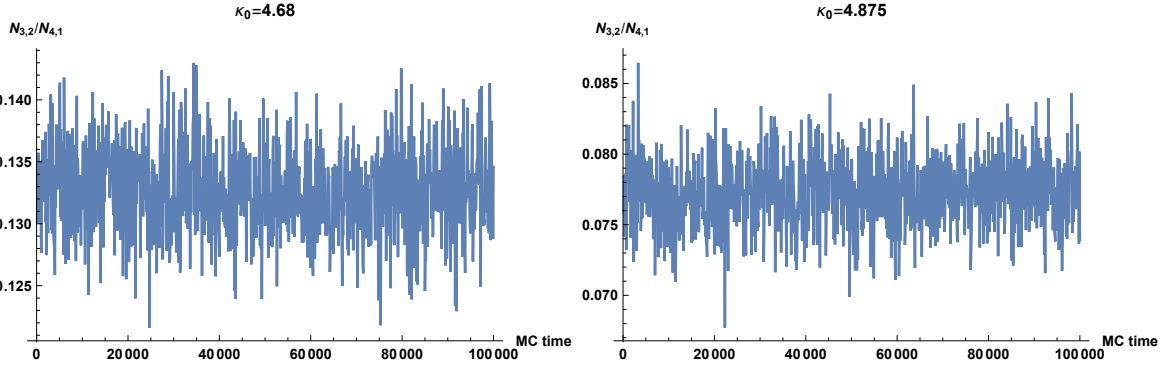


Figure 34: Monte Carlo time history of $OP_2 \equiv N_{3,2}/N_{4,1}$ at pseudo-critical points measured using the susceptibility method: $\kappa_0 = 4.68$ (left chart) and using the Binder cumulant method: $\kappa_0 = 4.875$ (right chart) for fixed $N_{4,1} = 200k$ and $T = 20$ time slices.

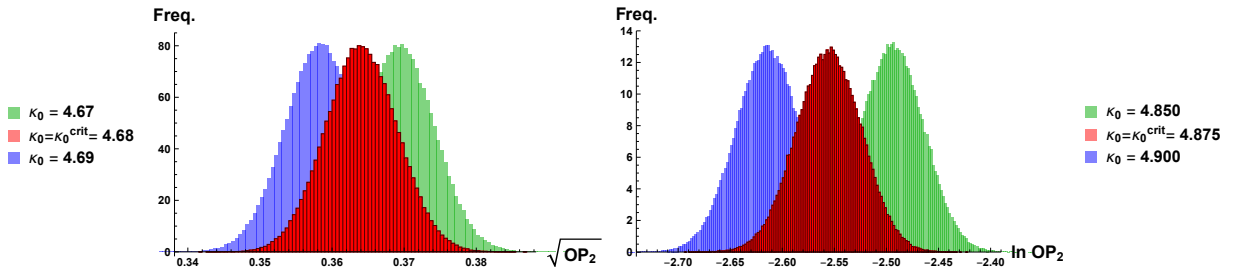


Figure 35: Exemplary histograms of the (functions of) order parameter $OP_2 \equiv N_{3,2}/N_{4,1}$ at pseudo-critical κ_0^{crit} values with fixed $N_{4,1} = 200k$ and $T = 20$ time slices. The left chart presents the histograms of $\sqrt{OP_2}$ measured in the vicinity of $\kappa_0^{crit} = 4.68$ based on the position of the susceptibility $\chi_{\sqrt{OP_2}}$ peak (Fig. 33, left), and the right chart shows the histograms of $\ln OP_2$ measured in the vicinity of $\kappa_0^{crit} = 4.875$ based on the position of the Binder cumulant B_{OP_2} minimum (Fig. 33, right). The histograms plotted in red are exactly at the transition points, while the green / blue data are for histograms measured for slightly lower / higher value of κ_0 than the critical value. The red, green and blue histograms overlap showing that the transition is smooth, allowing no space for the existence of any more than one state at the transition point.

4.2.3 Fixed $N_{4,1} = 200k$ ($T = 40$)

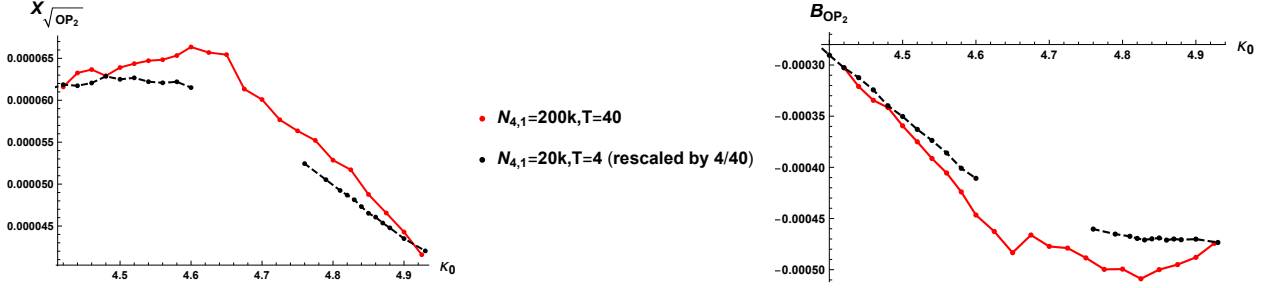


Figure 36: The susceptibility $\chi_{\sqrt{OP_2}} \approx \frac{\chi_{OP_2}}{\langle OP_2 \rangle}$ as defined by Eq. (3) (left chart) and the Binder cumulant B_{OP_2} as defined by Eq. (5) (right chart) as a function of κ_0 measured for fixed $N_{4,1} = 200k$ and $T = 40$ time slices (red line) and rescaled data for fixed $N_{4,1} = 20k$ and $T = 4$ time slices (black-dashed lines).

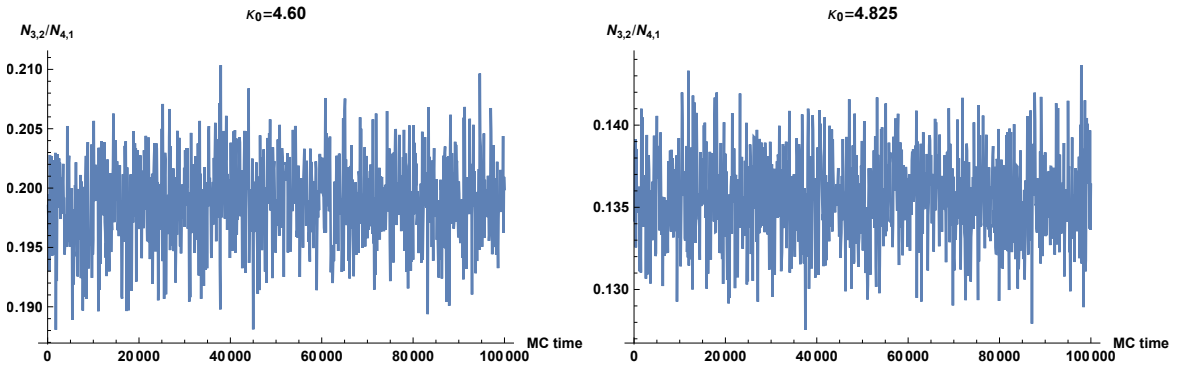


Figure 37: Monte Carlo time history of $OP_2 \equiv N_{3,2}/N_{4,1}$ at pseudo-critical points measured using the susceptibility method: $\kappa_0 = 4.60$ (left chart) and using the Binder cumulant method: $\kappa_0 = 4.825$ (right chart) for fixed $N_{4,1} = 200k$ and $T = 40$ time slices.

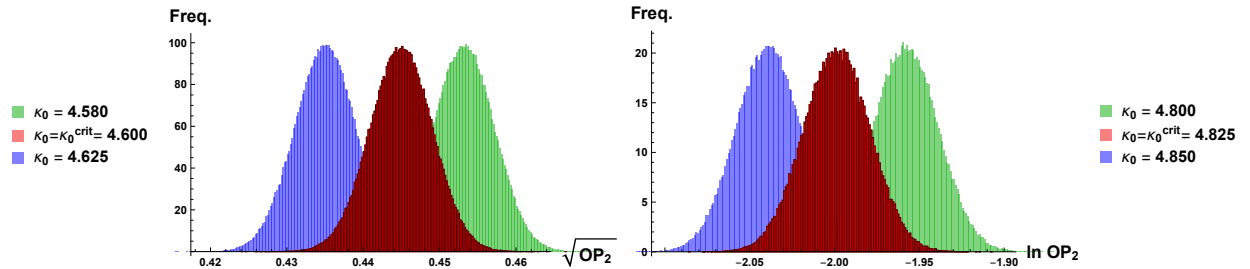


Figure 38: Exemplary histograms of the (functions of) order parameter $OP_2 \equiv N_{3,2}/N_{4,1}$ at pseudo-critical κ_0^{crit} values with fixed $N_4 = 200k$ and $T = 40$ time slices. The left chart presents the histograms of $\sqrt{OP_2}$ measured in the vicinity of $\kappa_0^{crit} = 4.60$ based on the position of the susceptibility $\chi_{\sqrt{OP_2}}$ peak (Fig. 36, left), and the right chart shows the histograms of $\ln OP_2$ measured in the vicinity of $\kappa_0^{crit} = 4.825$ based on the position of the Binder cumulant B_{OP_2} minimum (Fig. 36, right). The histograms plotted in red are exactly at the transition points, while the green / blue data are for histograms measured for slightly lower / higher value of κ_0 than the critical value. The red, green and blue histograms overlap showing that the transition is smooth, allowing no space for the existence of any more than one state at the transition point.

4.3 Impact of the volume fixing method

In this section we will investigate what impact, if any, the choice of the volume fixing method has on the properties of the $A-C$ transition in toroidal CDT. As before, we will focus especially on the Monte Carlo time history analysis of histograms measured at the transition points. It is known from [14] that the choice of volume fixing can affect the occurrence of metastable states at the $B - C_b$ transition. Fixing N_4 led to a Monte Carlo time history where configurations could jump between phase B configurations and phase C_b configurations. If we fixed $N_{4,1}$ we would see no such jumps. Thus naively one could be led to the conclusion that a N_4 volume fixing was associated with a first order transition while a $N_{4,1}$ volume fixing was associated with a second order transition. Closer analysis revealed that both volume fixings were associated with second order transitions, although it indeed is somewhat unusual that one observes metastable states (which weakens for larger volumes) for a second order transition. In the case of spherical spatial topology we have seen clear double peaks and other characteristics of a first order $A - C$ transition, as reported above, both in the case where N_4 was fixed and in the case where $N_{4,1}$ was fixed. Here we are now facing the opposite situation. In the case of the torus with $N_{4,1}$ fixed we have presented strong evidence above that the transition is still first order, but we saw no evidence of double peaks and metastable states at the transition point. Inspired by the situation at the $B - C_b$ transition we now want to fix N_4 instead of $N_{4,1}$ and see if that triggers the appearance of double peaks and metastable states.

4.3.1 Changing global volume fixing: fixed $N_4 = 160k$ ($T = 4$)

We start by keeping the number of time slices fixed at $T = 4$ and we change the volume fixing method to that of the total number of four-simplices fixed at $N_4 = 160k$. We again locate the pseudo-critical κ_0^{crit} values by either looking at the susceptibility $\chi_{\sqrt{OP_2}}$ maximum or at the Binder cumulant B_{OP_2} minimum, as shown in Fig. 39. The Monte Carlo time history of $OP_2 \equiv N_{3,2}/N_{4,1}$ at the transition points located using both methods is shown in Fig. 40 and the histograms measured at the transition points κ_0^{crit} and the neighbouring κ_0 values are presented in Fig. 41. We also analysed the histograms at all other measured κ_0 data points. In each case a single Gaussian-like behaviour was observed and the evolution of the OP_2 parameter was smooth without exhibiting any metastable state switching.

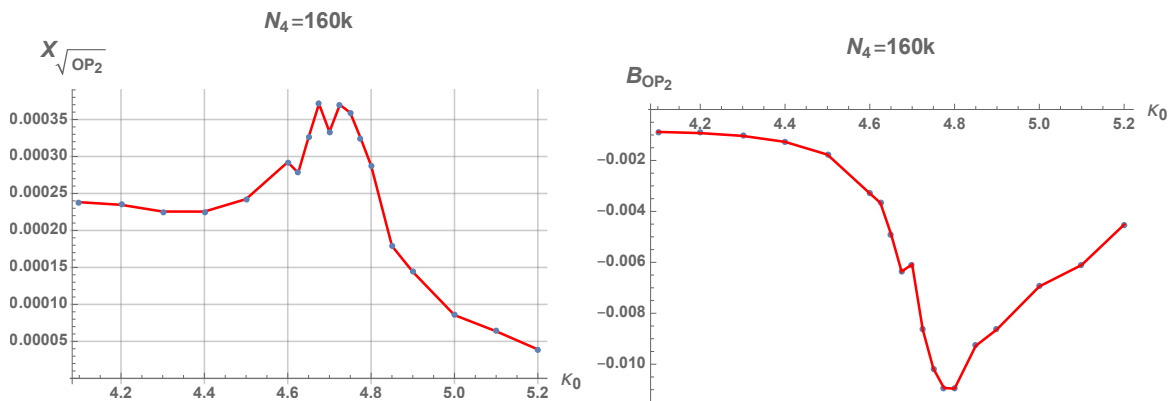


Figure 39: The susceptibility $\chi_{\sqrt{OP_2}} \approx \frac{\chi_{OP_2}}{\langle OP_2 \rangle}$ as defined by Eq. (3) (left chart) and the Binder cumulant B_{OP_2} as defined by Eq. (5) (right chart) as a function of κ_0 for fixed $N_4 = 160k$ and $T = 4$ time slices.

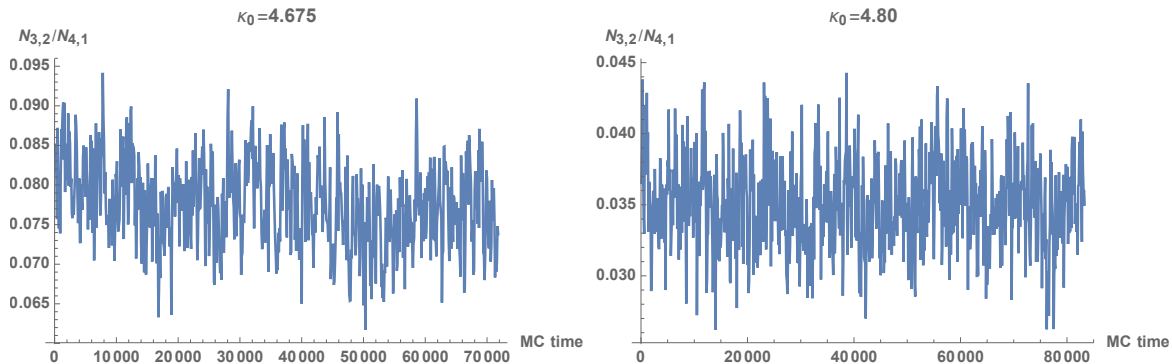


Figure 40: Monte Carlo time history of $OP_2 \equiv N_{3,2}/N_{4,1}$ at pseudo-critical points measured using the susceptibility method: $\kappa_0 = 4.675$ (left chart) and using the Binder cumulant method: $\kappa_0 = 4.80$ (right chart) for fixed $N_4 = 160k$ and $T = 4$ time slices.

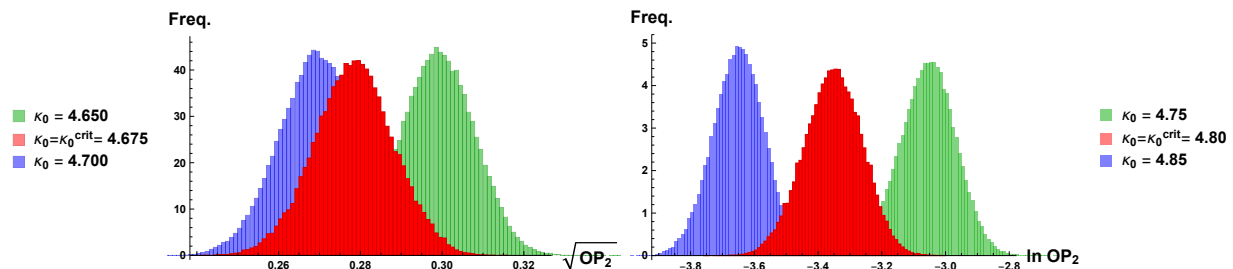


Figure 41: Exemplary histograms of the (functions of) order parameter $OP_2 \equiv N_{3,2}/N_{4,1}$ at pseudo-critical κ_0^{crit} values with fixed $N_4 = 160k$ and $T = 4$ time slices. The left chart presents the histograms of $\sqrt{OP_2}$ measured in the vicinity of $\kappa_0^{crit} = 4.675$ based on the position of the susceptibility $\chi_{\sqrt{OP_2}}$ peak (Fig. 39, left), and the right chart shows the histograms of $\ln OP_2$ measured in the vicinity of $\kappa_0^{crit} = 4.8$ based on the position of the Binder cumulant B_{OP_2} minimum (Fig. 39, right). The histograms plotted in red are exactly at the transition points, while the green / blue data are for histograms measured for slightly lower / higher value of κ_0 than the critical value. The red, green and blue histograms overlap showing that the transition is smooth, allowing no space for the existence of any more than one state at the transition point.

4.3.2 Adding a local volume fixing term ($T = 40$)

So far we were not able to observe any jumping between metastable states for the $A-C$ transition in the case of toroidal spatial topology, while such jumping is clearly visible in the spherical topology case. The obvious difference between the two topologies lies in the shape of the CDT spatial volume profile in phase C , which is non-trivial, i.e. $\langle n_t \rangle \propto \cos^3(t/t_0)$, in the spherical case and is trivial, i.e. $\langle n_t \rangle = const.$, in the toroidal case (see Fig. 42). One reason that we have not been able to observe distinctly different metastable states at the transition point could be that the dominant “semiclassical” configuration in phase C in the case of toroidal spatial topology looks too similar to configurations in phase A . So, in order to try to force the configurations in phase C to look more like the non-trivial, dominant configuration in the case of spherical topology, we simply impose a non-trivial spatial volume n_t dependence in the toroidal case. As discussed in detail in Ref. [24] this can be done by performing numerical MC simulations with a nontrivial local volume-fixing term:

$$\delta V^{local} = \epsilon [(n_1 - \hat{n}_1)^2 + (n_h - \hat{n}_h)^2] , \quad (20)$$

which makes the spatial volume of two chosen slices, namely n_1 and n_h , fluctuate around \hat{n}_1 and \hat{n}_h , respectively. Due to the imposed time-periodic boundary conditions it is convenient to choose $h = T/2 + 1$. In the following we will describe the results obtained for fixed $N_{4,1} = 160k$, $\hat{n}_1 = 1k$, $\hat{n}_h = 7k$ and $T = 40$ time slices, resulting in $h = T/2 + 1 = 21$. We can say that if the toroidal system does not at all have a tendency to form a non-trivial spatial distribution, we impose a “boundary” condition which should encourage it to form such a distribution (much like using a boundary condition for a spin system which encourage the spin to point up rather than down). However, as seen in Fig. 43, it only takes a few steps in the time direction for the configurations to get back to the constant configuration shown in Fig. 42.

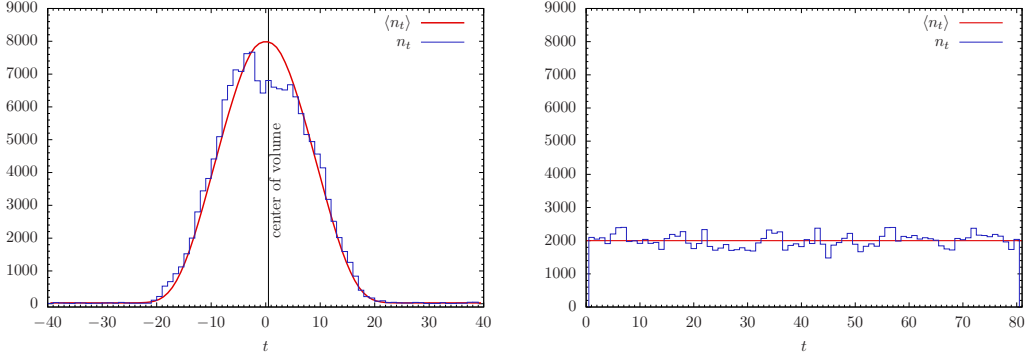


Figure 42: The average (red) and typical (blue) volume profiles for the spherical spatial topology (left chart) and for the toroidal spatial topology (right chart) deep inside the phase C ($\kappa_0 = 2.2$, $\Delta = 0.6$) in CDT with $N_{4,1} = 160k$ volume fixed and $T = 80$ time slices.

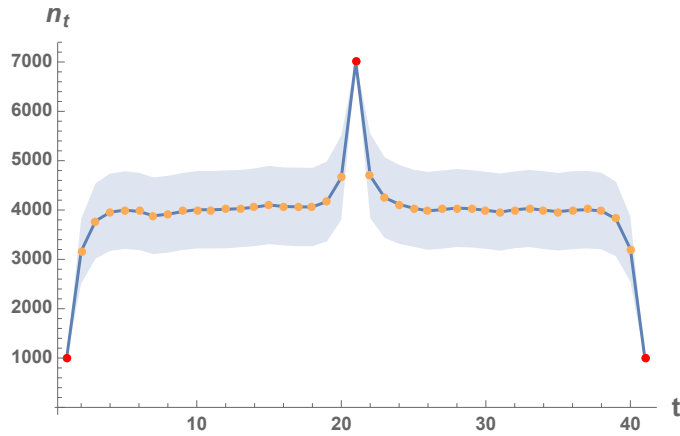


Figure 43: The spatial volume profile measured for bare coupling constants $\kappa_0 = 4.54$, $\Delta = 0.6$ and time period $T = 40$ in toroidal CDT with fixed $N_{4,1} = 160k$ and also local volume fixing (20). Red dots denote time slices with fixed local volume $\hat{n}_1 = 1k$ and $\hat{n}_h = 7k$, $h = T/2 + 1 = 21$. The average spatial volume $\langle n_t \rangle$ is plotted as orange points linked by a blue solid line, the amplitude of fluctuations $\langle n_t \rangle \pm \Delta n_t$, $\Delta n_t = \sqrt{\langle (n_t - \langle n_t \rangle)^2 \rangle}$ is shown as the shaded region.

We again repeat the analysis of Subsection 4.3.1 by locating the pseudo-critical κ_0^{crit} values looking for susceptibility $\chi_{\sqrt{OP_2}}$ peaks (see Fig. 44). The Monte Carlo time history of $OP_2 \equiv N_{3,2}/N_{4,1}$ at the transition point is shown in Fig. 45 and the $\sqrt{OP_2}$ histogram is presented in Fig. 46. At the transition point, and also for all other measured κ_0 data points, one observes a

single Gaussian-like behaviour of the OP_2 parameter. In view of the short range distortions of the volume profile shown in Fig. 43 this is not surprising. However, we also have to conclude that in the case of toroidal spatial topology we have no natural geometric interpretation of the first order transition. It might be that the systems we consider are simply too small to be able to observe OP_2 histograms with two distinct peaks, as we have already discussed¹⁵, or it might be that this phase transition is atypical for a first order transition (like the $B - C_b$ transition was atypical for a second order transition).

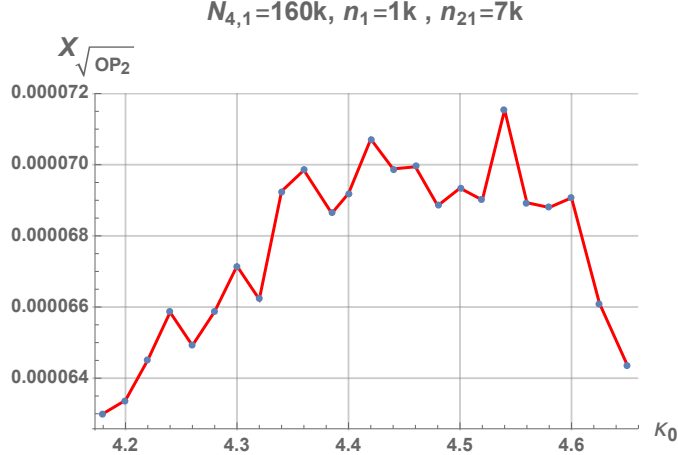


Figure 44: The susceptibility $\chi_{\sqrt{OP_2}} \approx \frac{\chi_{OP_2}}{\langle OP_2 \rangle}$ as defined by Eq. (3) as a function of κ_0 in toroidal CDT with $T = 40$ time slices and with fixed $N_{4,1} = 160k$ and also local volume fixing $n_1 = 1k$ and $n_{21} = 7k$.

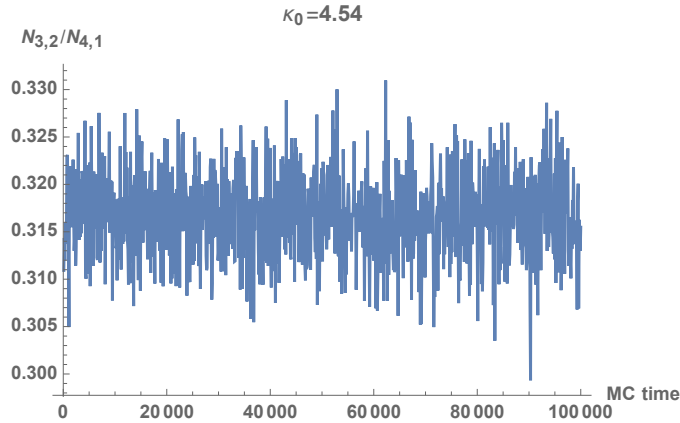


Figure 45: Monte Carlo time history of $OP_2 \equiv N_{3,2}/N_{4,1}$ at pseudo-critical point $\kappa_0^{crit} = 4.54$ measured using the susceptibility peak method (see Fig. 44) in toroidal CDT with $T = 40$ time slices and with fixed $N_{4,1} = 160k$ and also local volume fixing $n_1 = 1k$ and $n_{21} = 7k$.

¹⁵Unfortunately, we were not able to observe the metastable state switching even for our biggest systems consisting of $N_{4,1} = 500k$ simplices, and, due to the exponentially growing thermalization time, we cannot go much further as regards the simulated system sizes.

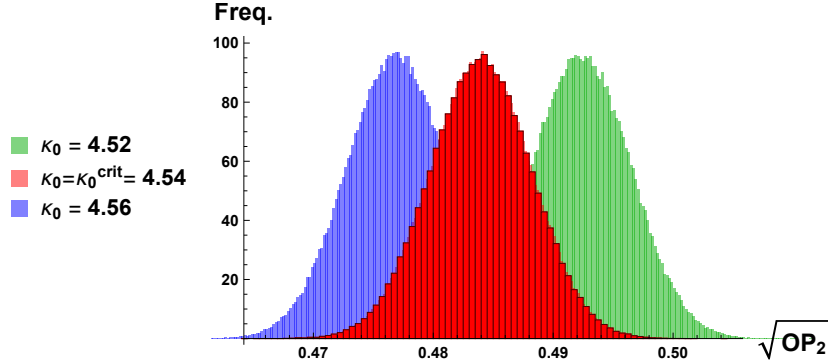


Figure 46: Exemplary histograms of $\sqrt{OP_2} \equiv \sqrt{N_{3,2}/N_{4,1}}$ at pseudo-critical $\kappa_0^{crit} = 4.54$ value in toroidal CDT with $T = 40$ time slices and with fixed $N_{4,1} = 160k$ and also local volume fixing $n_1 = 1k$ and $n_{21} = 7k$. The histogram plotted in red is exactly at the transition point measured using the susceptibility peak method (see Fig. 44), while the green / blue data are for histograms measured for a slightly lower / higher value of κ_0 than the critical value. The red, green and blue histograms overlap showing that the transition is smooth, allowing no space for the existence of any more than one state at the transition point.

4.4 Summary of the toroidal topology

Summing up this part, using the $OP_2 \equiv N_{3,2}/N_{4,1}$ order parameter we have analysed in detail the $A-C$ transition for a system with toroidal spatial topology, $T = 4$ time slices and $N_{4,1}$ volume fixing. We have confirmed two of three signatures of the first order transition (see Table 1), namely the shift exponent γ consistent with one, and scaling of the Binder cumulant $B_{OP_2}^{min}$, which diverges from zero when the lattice volume is increased. Unfortunately, we were not able to observe OP_2 histograms with two distinct peaks. We have then checked the impact of the number of time slices used in numerical Monte Carlo simulations and we found universal scaling relations of $\langle OP_2 \rangle$ and χ_{OP_2} with the lattice volume $N_{4,1}$ and T , suggesting that the OP_2 can be modelled as an average of T statistically independent identical random variables $\widetilde{OP}_2(n_t)$, dependent only on $\langle n_t \rangle = N_{4,1}/T$. This kind of behaviour is indeed expected inside phase A , where one can show that triangulations consist of T independent (or at least uncorrelated) time slices, but, surprisingly, it also seems to hold (at least not too deep) inside phase C , where various time slices are correlated [23]. The study led to the scaling relation of Eq. (19) which strongly supports the first order nature of the $A - C$ transition. Finally, we have investigated the impact of the volume fixing method, either by changing the global volume fixing to that of N_4 fixed, or by adding a local volume fixing term yielding a non-trivial spatial volume dependence. Unfortunately, in none of the cases were we able to observe the metastable state switching at the $A - C$ transition points during our Monte Carlo runs. We suspect that this is caused by much larger finite size effects in CDT with the toroidal spatial topology, compared to the spherical topology case.

5 Discussion and conclusions

We have investigated the $A - C$ phase transition in CDT with spherical and toroidal spatial topology. For the spherical topology, fixing the number of $N_{4,1}$ simplices and keeping the number of time slices at $T = 80$ we have determined the pseudo-critical κ_0 value for 8 different lattice volumes, finding a shift exponent of $\gamma = 1.16 \pm 0.07$ that strongly supports the first order nature

of the $A-C$ transition. This finding is further supported by calculations of the Binder cumulant, which is found to move away from zero with increasing lattice volume, which also suggests a first order transition. In the case of spherical topology, a double peaked histogram appears at pseudo-critical transition points regardless of the particular volume fixing method, namely it does not seem to matter whether one fixes the total number of simplices N_4 or just the number of $N_{4,1}$ simplices. Varying the number of time slices between $T = 80$ and $T = 4$ at the pseudo-critical κ_0 value has a noticeable impact. Namely, for $T = 4$ we can not verify the presence of a double peak structure in the histogram data up to a resolution of three decimal places in κ_0 . However, an analysis of the Monte Carlo time evolution either side of the putative transition suggests a double peak structure is likely to emerge for a greater resolution of κ_0 . This is the consequence of the very sharp separation of the states at both sides of the transition, further supporting the first order nature of the $A - C$ transition, consistent with the earlier finding of ref. [17].

For toroidal topology, fixing the number of $N_{4,1}$ simplices and keeping the number of time slices at $T = 4$ we have determined the pseudo-critical κ_0 value for 11 different lattice volumes, finding a shift exponent of $\gamma = 1.22 \pm 0.08$, also consistent with the first order transition. We have also investigated the Binder cumulant, which is found to move away from zero with increasing lattice volume, also supporting the first order nature of the transition. We were not able to observe double peaks in histograms of the order parameter measured at the transition points. Varying the number of time slices or changing the volume fixing method also does not lead to the metastable state switching during Monte Carlo simulations at the transition points in toroidal CDT. A detailed analysis of the scaling of susceptibility at the transition points leads to the discovery of the universal scaling relation (19):

$$\chi_{N_{3,2}}^{crit} = \chi^* \cdot N_{4,1} , \quad \chi^* = const. ,$$

independent of the number of time slices T and valid for any lattice volume $N_{4,1}$. Such a scaling, observed for finite lattices, typically translates into delta-like singularities of susceptibility in the infinite volume limit, thus strongly supporting the first order nature of the $A - C$ transition in toroidal CDT.

Although the $A - C$ transition seems to be much smoother for toroidal CDT, and therefore one couldn't observe the metastable state separation at the transition points, this might be attributed to much larger finite size effects for toroidal topology compared to spherical topology. Therefore, all our results strongly suggest that the volume fixing method, the number of time slices used in the Monte Carlo simulations and the chosen topology of spatial hypersurfaces of equal global proper time coordinates do not have an impact on the nature of the $A - C$ transition. Thus the behaviour is very universal.

Acknowledgements

JGS acknowledges support from the grant UMO-2016/23/ST2/00289 from the National Science centre, Poland. JA and DC acknowledge support from the Danish Research Council grant *Quantum Geometry*. AG acknowledges support by the National Science Centre, Poland, under grant no. 2015/17/D/ST2/03479.

References

- [1] G. 't Hooft and M. J. G. Veltman,
One loop divergencies in the theory of gravitation,
Ann. Inst. H. Poincare Phys. Theor. A **20** (1974) 69.
- [2] M. H. Goroff and A. Sagnotti,
The Ultraviolet Behavior of Einstein Gravity,
Nucl. Phys. B **266** (1986) 709. doi:10.1016/0550-3213(86)90193-8
- [3] S. Weinberg,
in *General Relativity: Einstein Centenary Survey*,
eds. S.W. Hawking and W. Israel (Cambridge University Press, Cambridge, UK, 1979) 790-831.
- [4] M. Reuter,
Nonperturbative evolution equation for quantum gravity,
Phys. Rev. D **57** (1998) 971-985 [hep-th/9605030].
A. Codello, R. Percacci and C. Rahmede,
Investigating the ultraviolet properties of gravity with a Wilsonian renormalization group equation,
Annals Phys. **324** (2009) 414 [arXiv:0805.2909, hep-th].
M. Reuter and F. Saueressig,
Functional renormalization group equations, asymptotic safety, and Quantum Einstein Gravity
arXiv:0708.1317, hep-th
M. Niedermaier and M. Reuter,
The asymptotic safety scenario in quantum gravity,
Living Rev. Rel. **9** (2006) 5.
D.F. Litim,
Fixed points of quantum gravity,
Phys. Rev. Lett. **92** (2004) 201301 [hep-th/0312114].
- [5] J. Ambjørn, J. Jurkiewicz and R. Loll,
Dynamically triangulating Lorentzian quantum gravity,
Nucl. Phys. B **610** (2001) 347, [hep-th/0105267].
Reconstructing the universe,
Phys. Rev. D **72** (2005) 064014 [hep-th/0505154].
Emergence of a 4-D world from causal quantum gravity,
Phys. Rev. Lett. **93** (2004) 131301 [hep-th/0404156].
J. Ambjørn, A. Görlich, J. Jurkiewicz and R. Loll,
The Nonperturbative Quantum de Sitter Universe,
Phys. Rev. D **78** (2008) 063544 [arXiv:0807.4481, hep-th];
Planckian Birth of the Quantum de Sitter Universe,
Phys. Rev. Lett. **100** (2008) 091304 [arXiv:0712.2485, hep-th].
- [6] J. Ambjorn, A. Görlich, J. Jurkiewicz and R. Loll,
Nonperturbative Quantum Gravity,
Phys. Rept. **519** (2012) 127 [arXiv:1203.3591, hep-th].

- [7] 5
- [8] T. Regge,
General Relativity Without Coordinates,
Nuovo Cim. **19** (1961) 558.
- [9] J. Ambjorn, J. Gizbert-Studnicki, A. Görlich, K. Grosvenor and J. Jurkiewicz,
Four-dimensional CDT with toroidal topology,
Nucl. Phys. B **922** (2017) 226, [arXiv:1705.07653 [hep-th]].
- [10] J. Ambjorn, D. N. Coumbe, J. Gizbert-Studnicki and J. Jurkiewicz,
Signature Change of the Metric in CDT Quantum Gravity?,
JHEP **1508** (2015) 033, [arXiv:1503.08580 [hep-th]].
- [11] D. N. Coumbe, J. Gizbert-Studnicki and J. Jurkiewicz,
Exploring the new phase transition of CDT,
JHEP **1602** (2016) 144, [arXiv:1510.08672 [hep-th]].
- [12] J. Ambjorn, D. Coumbe, J. Gizbert-Studnicki and J. Jurkiewicz,
Recent results in CDT quantum gravity,
doi:10.1142/9789813226609-0516 [arXiv:1509.08788 [gr-qc]].
- [13] J. Ambjorn, D. Coumbe, J. Gizbert-Studnicki, A. Gorlich and J. Jurkiewicz,
New higher-order transition in causal dynamical triangulations,
Phys. Rev. D **95** (2017) no.12, 124029, [arXiv:1704.04373 [hep-lat]].
- [14] J. Ambjorn, J. Gizbert-Studnicki, A. Görlich, J. Jurkiewicz, N. Klitgaard and R. Loll,
Characteristics of the new phase in CDT,
Eur. Phys. J. C **77** (2017) no.3, 152, [arXiv:1610.05245 [hep-th]].
- [15] D. N. Coumbe and J. Jurkiewicz,
Evidence for Asymptotic Safety from Dimensional Reduction in Causal Dynamical Triangulations, JHEP **1503** (2015) 151, [arXiv:1411.7712 [hep-th]].
- [16] J. Ambjorn, S. Jordan, J. Jurkiewicz and R. Loll,
A Second-order phase transition in CDT,
Phys. Rev. Lett. **107** (2011) 211303 [arXiv:1108.3932 [hep-th]].
- [17] J. Ambjorn, S. Jordan, J. Jurkiewicz and R. Loll,
Second- and First-Order Phase Transitions in CDT,
Phys. Rev. D **85** (2012) 124044, [arXiv:1205.1229 [hep-th]].
- [18] J. Ambjorn, D. Coumbe, J. Gizbert-Studnicki and J. Jurkiewicz,
Searching for a continuum limit in causal dynamical triangulation quantum gravity,
Phys. Rev. D **93** (2016) no.10, 104032, [arXiv:1603.02076 [hep-th]].
- [19] J. Ambjørn, A. Görlich, S. Jordan, J. Jurkiewicz and R. Loll,
CDT meets Horava-Lifshitz gravity,
Phys. Lett. B **690** (2010) 413, [arXiv:1002.3298, hep-th].

- [20] P. Hořava,
Quantum gravity at a Lifshitz point,
 Phys. Rev. D **79** (2009) 084008 [arXiv:0901.3775, hep-th].
General Covariance in Gravity at a Lifshitz Point,
 Class. Quant. Grav. **28** (2011) 114012, [arXiv:1101.1081, hep-th].
- [21] K. Binder,
 Z. Phys. B 43, 119 (1981); Phys.Rev. Lett. 47, 693 (1981).
 K. Binder, D. W. Heermann,
Monte Carlo Simulation in Statistical Physics: An Introduction,
 (2010) Springer
- [22] J. Ambjorn, J. Gizbert-Studnicki, A. Görlich, J. Jurkiewicz and D. Nèmeth,
The phase structure of Causal Dynamical Triangulations with toroidal spatial topology,
 JHEP **1806** (2018) 111, [arXiv:1802.10434 [hep-th]].
- [23] J. Ambjorn, Z. Drogosz, J. Gizbert-Studnicki, A. Görlich, J. Jurkiewicz and D. Nemeth,
Impact of topology in causal dynamical triangulations quantum gravity,
 Phys. Rev. D **94** (2016) no.4, 044010, [arXiv:1604.08786 [hep-th]].
- [24] J. Ambjorn, J. Gizbert-Studnicki, A. Görlich, K. Grosvenor and J. Jurkiewicz,
Four-dimensional CDT with toroidal topology,
 Nucl. Phys. B **922** (2017) 226, [arXiv:1705.07653 [hep-th]].